Modelling of OBS Data Across the Vestbakken Volcanic Province

Asude Arslan Sørensen

Master Thesis

Department of Earth Science

University of Bergen

June 2011

ABSTRACT

A P-Wave model of a 384 km long Ocean Bottom Seismometer profile has been modelled by use of ray-tracing. The profile, Bear Island South (BIS-2008), crossses the transtensional Vestbakken Volcanic Province and the boundary between northern Atlantic oceanic crust of the Barents Sea continental platform. This study is a part of the 4th International Polar Year (IPY) international project entitled 'The Dynamic Continental Margin Between the Mid-Atlantic-Ridge (Mohns Ridge, Knipovich Ridge) and the Bear Island Region'. The thickness of crust varies greatly along the profile, from 7 km at the oceanic part (southwest) to approximately 32 km at the continental part (northeast). Northeastern part of the profile represents continental crust and southwestern part shows the oceanic crust. The transition from oceanic crust to continental crust occurs in a narrow zone of 30 km width. The continent ocean boundary (COB) is located in the range 190-220 km along the profile. The Hornsund and Knølegga fault zones are modelles as significant lateral variations in velocity.

Acknowledgements

I would like to thank my supervisor, Professor Rolf Mjelde, for an interesting project, good supervision, quick replies and very helpful feedbacks. I would also like to thank Audun Libak for showing me how to use the programs and very good discussions.

I would like to express my gratitude for my mum for her support.

Finally, thanks to my husband, Martin Sørensen; your encouragement and belief in me throughout these years have meant the world to me.

Asude Arslan Sørensen
Bergen, June 2011

1. INTRODUCTION

The Barents Sea shelf extends over a large area from the Arctic coasts of Norway and Russia to the Arctic Ocean margins (Worsley et. al., 2001). Hydrocarbon exploration has shown a complex structural development, with several major subprovinces containing sedimentary successions from Upper Palaeozoic to Cenozoic times (Rønnevik et al. 1982; Rønnevik & Jacobsen 1984; Faleide et al. 1984; Johansen et al. 1992; Nøttvedt et al. 1992; Gudlaugsson et al. 1998). The study area of this thesis is the Norwegian-Greenland Sea and the South Western Barents Sea margin (Figure 1.1). Several studies have focused on this area the last decade. However, since the magnetic anomalies of the oceanic crust are diffuse and difficult to identify, the spreading history of the ridge is therefore poorly understood.

Bjørnøya (Bear Island) is a small island of 178km^2 located on the Stappen High, western Barents Sea, between Svalbard and Norway. Bjørnøya forms the highest point of Stappen High, which was a positive structure in Late Palaeozoic, then subsided in the Mesozoic and finally, was uplifted in the Cenozoic times (Worsley et. al., 2001).

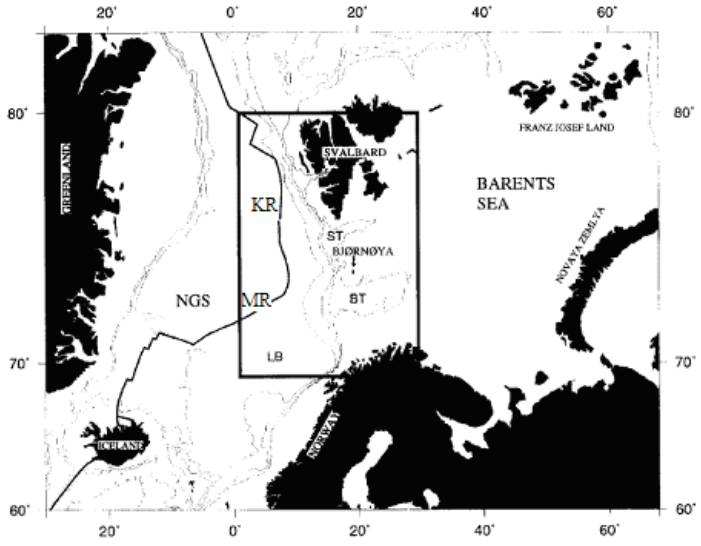

Figure 1. 1. Southwestern Barents sea, BT = Bjørnøya Trough, KR = Knipovich Ridge, LB = Lofoten Basin, MR = Mohns Ridge, NGS = Norwegian-Greenland Sea, ST = Storfjorden Trough. (Faleide et al., 1995).

A seismic wide angle reflection and refraction profile was done in the International Polar Year Project (IPY), "The dynamic continental margin between the Mid-Atlantic Ridge (Knipovich and Mohns Ridge) and the Bear Island region". Ocean Bottom Seismometers (OBS) may provide better understanding of the spreading history when there is absence of magnetic anomalies. In addition, OBS give better knowledge about the tectonic structure and composition by using the refraction seismic method. This thesis presents the results from an OBS refraction experiment conducted in 2008 from the Bear Island crossing the transtensional Vestbakken Volcanic Province. Fifteen three-component OBSs were deployed along the profile BIS-2008 (Bear Island-South) (Figure 1.2). The distance between the OBSs are 16 km, which is the shortest OBS distance in the area up to date.

The main aim of this thesis is to form a crustal scale P-wave velocity for the area covered by BIS-Profile. In order to find out more about the geology of the area the model will be interpreted. By using the interpreted model, the tectonic evolution of the southwestern Barents Sea and the Bear Island will be discussed.

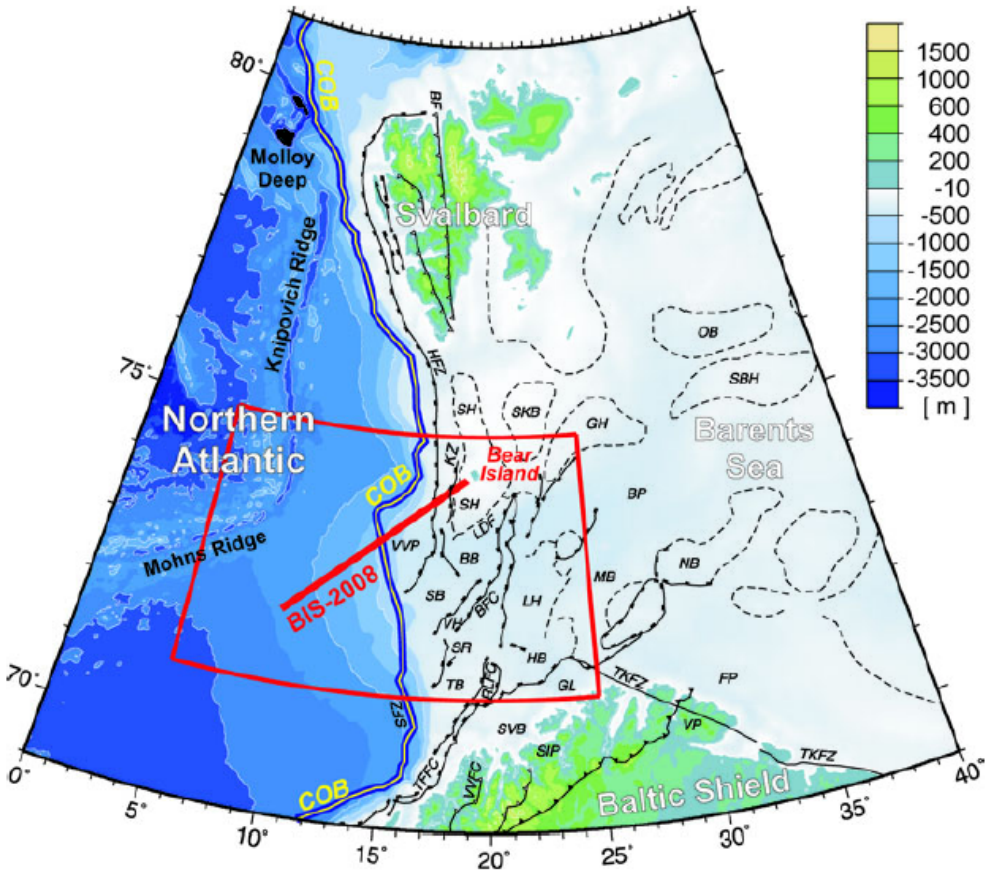

Figure 1. 2. BIS-Profile (red line) with the surrounding tectonic features (Mohns Ridge-Bear Island) on the background of topography/bathymetry map (Jakobsson et al. 2000). The tectonic elements were simplified by Gabrielsen et al., 1990 and Faleide et al., 2008. COB= Continent Ocean Boundary (Breivik et al. 1999); BB= Bjørnøya Basin; BFC= Bjørnøyrenna Fault Complex; FP= Finnmark Platform; GH= Gardarbanken High; HB= Hammerfest Basin; HFZ= Hornsund Fault Zone; KF= Knølegga Fault; LDF= Leirdjupet Fault; LH= Loppa High; NB= Nordkapp Basin; SB= Sørvestsnaget Basin; SH= Stappen High; SKB= Sørkap Basin; SFZ= Senja Fracture Zone; SR= Senja Ridge; TB= Tromsø Basin; VVP= Vestbakken Volcanic Province (Czuba et. al., 2011).

2. CONTINENTAL and OCEANIC CRUST

The top layer of the Earth is called crust, which is typically 40-60 km thick beneath continents, 25 km thick on stretched crust and about 7 km thick beneath oceans. It is divided into two distinct types; continental and oceanic crust.

2.1. Continental Crust

Continental crust is found beneath continents and is bounded by the Moho discontinuity. The crust is highly heterogeneous, and can be explained by a three layer model differing by seismic velocities and composition. The upper (5.7-6.4 km/s), middle (6.4 - 6.8 km/s) and the lower crust (6.8 - 7.6 km/s), is the most common definition of layered continental crust.

Sedimentary rocks generally form the uppermost layer of continental crust. Then comes crystalline crust which often is divided into three as; felsic upper crust, middle crust and more mafic lower crust. Layered sequences of felsic and mafic rocks are observed as strong seismic reflectivity in many regions in the lower crust (Artemieva, 2001).

For an average 40 km thick continental crust, the middle crust has a thickness of 11 km from 12 km to 23 km depth (Rudnick and Fountain, 1995), whereas the lower crust has an average thickness of 17 km, beginning at a depth of 23 km.

Both the thickness and depth of lower and middle crusts change according to geological settings. For example, the middle and lower crusts are generally thin in tectonically active rifted margins. The crust is much thicker in Mesozoic-Cenozoic orogenic belts. The lower crust can be up to 25 km thick (Rudnick and Fountain, 1995). Geologic studies have shown that the continental crust becomes more mafic and denser with depth.

2.1. Oceanic Crust

The oceanic crust is thinner than the continental crust. Seismic refraction studies have shown that it is 6-7 km thick under an average water depth of 4.5 km. In areas where the magma supply rate is very high due to higher than normal temperatures in the

mantle, the crust is thicker (White and Mckenzie, 1989). When it is compared with continental crust, the maximum age of oceanic crust is about 200 years and it is continuously being created at mid-ocean ridges.

The oceanic crust generally consists of three layers. Layer 1; which is the top layer has a thickness from 0.1 to 1.0 km of unconsolidated sediments. It thickens progressively away from the ocean ridges where it is very thin or not exists. The volcanic and faulted nature of layer 2 causes a more rugged interface between layer 1 and layer 2 than at the seabed (Figure 2.2).

Layer 2 varies in thickness from 1.0 to 2.5 km and the seismic velocity increases with depth from 3.4 to 6.2 km/s. The layer is the uppermost part of the magmatic crust, and it consists of extrusive igneous material (Sun et al, 1979). Layer 2 has three subdivisions (Figure 2.2). Sublayer 2A is only seen on ocean ridges near eruptive centers in areas which are effected by hydrothermal circulation of sea water. It consists of porous fresh basalts and its thickness varies between 0 and 1 km and the velocity is below 4.8 km/s. Sublayer 2B has lower porosity and higher velocity than sublayer 2A. It is a basaltic layer, mostly dikes which has a velocity between 4.8 km/s and 5.5 km/s. By the infilling of pores by secondary minerals as calcite, quartz and zeolites, sublayer 2A can be converted to sublayer 2B with time. Layer 2C has velocities of 5.8-6.2 km/s and if it is present, it is approximately 1km thick (Kearey and Vine, 1996). The layer includes high proportion of intrusive mafic rocks.

Layer 3 is the main component of oceanic crust (Stroup and Fox, 1981). This layer forms as a result of crystallization of magma chamber(s), with an upper layer, sublayer 3A, of isotropic gabbros. Lower layer, sublayer 3B, consists of cumulate gabbro and ultramafic rocks from crystal settling (Auzende et. al., 1989). Sublayer 3A is up to 3 km thick and the velocity varies from 6.5 to 6.8 km/s. Layer 3B is 1-2 km thick and has a velocity from 7.0 to 7.7 km/s.

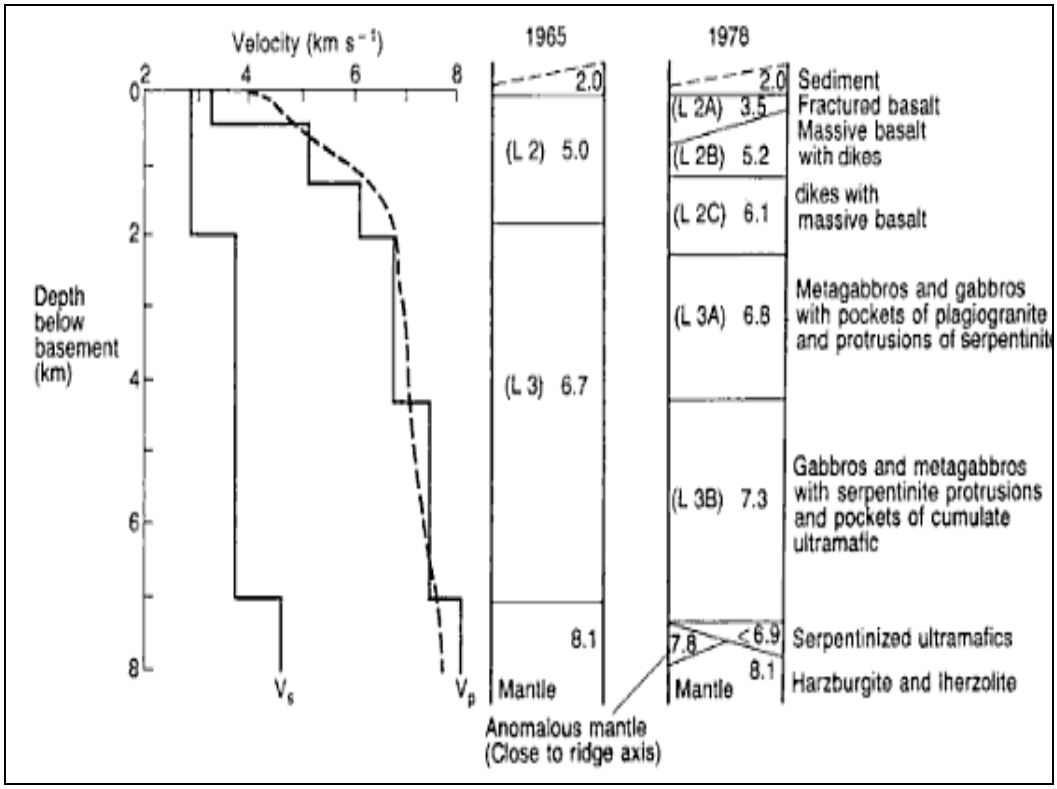

Figure 2. 2. P- and S-wave velocity of oceanic crust and layered models. Gradational increase in velocity with depth shown with dashed lines (Spudich & Orcutt J, 1980; Harrison & Bonatti, 1981; Kearey & Vine, 1996; White et. al., 1992)

2.3. Mid-Ocean Ridges

The global mid-ocean ridge system is the largest single volcanic feature on Earth where Earth's crust is spreading, creating oceanic crust and literally renewing the surface of our planet. Mid-Ocean Ridges consist of thousands of individual volcanoes or volcanic ridge segments that erupt periodically. They are formed as a result of two plates pulling apart from each other while hot magma from the mantle fills the cracks continuously created by plate separation. The magmatic flow then moves horizontally away from the ridge. After the cooling of lava, it attaches itself to the edge of each plate, forming oceanic crust. This process is known as sea-floor spreading. The driving mechanisms of these movements are convection currents in sub-lithospheric mantle (Macdonald et. al., 1995).

Ocean ridges have been divided into fast-, intermediate-, and slow-spreading based on their spreading rates (Figure 2.3). Slow rates are 10 - 50mm a^{-1}, and such ridges are found in the Mid-Atlantic and Indian Ocean. They are generaly 30 to 50 km wide and 1500 - 3000 m deep with rugged topography.

Intermediate ridges have a spreading rate of 50 - 90 mm a^{-1}, such as at the Galapagos spreading center and the most northerly East Pacific Rise. The median rift at intermediate spreading centers is 50 - 200 m deep and they have a relatively smooth topography.

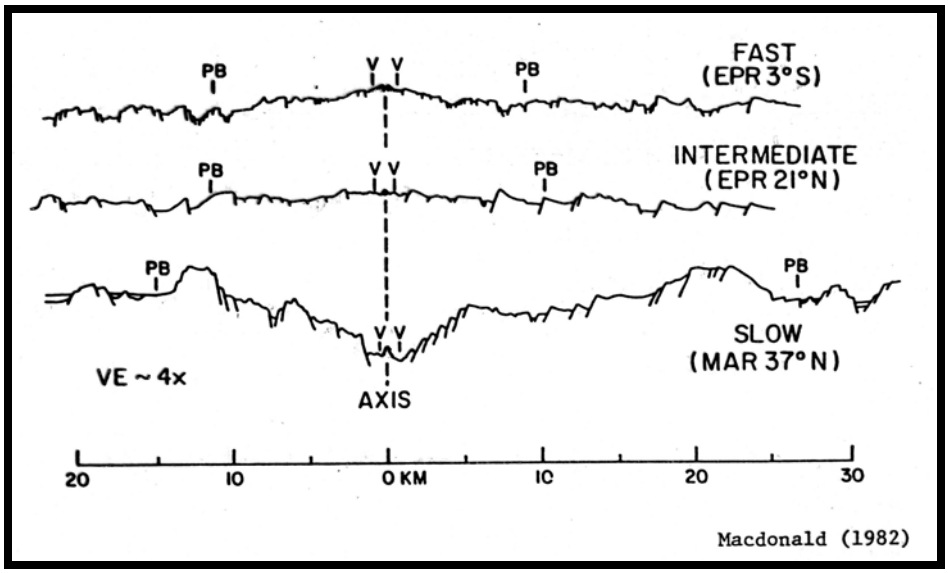

Figure 2. 3. Fast, intermediate and slow spreading rates at mid-oceanic ridges. Above, East Pasific Rise, Middle East Pasific Rise, Below Mid-Atlantic Ridge (MacDonald 1982; Kearey and Vine 1996).

At fast spreading ridges, the spreading rate is greater than 90 mm a^{-1}. Along such ridges, there is no median rift and the topography is relatively smooth.

In addition to fast-, intermediate-, and slow-spreading ridges, there is also one more ridge type which is called ultraslow spreading ridge. Their spreading rate is less then 20 mm per year. Most of the ultraslow spreading ridges are found in polar or near-polar regions, including the circum-antarctic plate boundary and the Arctic spreading system. The studies of ultraslow-spreading ridges have shown several anomalies that

can not be explained by the standard model of oceanic crustal formation. For that reason, in the last decade, ultraslow-spreading ridges have started to be recognized as a class in themselves.

Ultraslow spreading ridges consist of magmatic and amagmatic accretionary ridge segments. Axial highs or troughs which are formed sub-perpendicularly to the direction of the least principal stress axes are magmatic segments (Dauteuil, O. and Brun, J. P.,1993). Amagmatic segments are a key component of ultraslow-spreading ridges. They are replacing transform faults at the same time as they are extending the lithospheric accretion zone. They accept any orientation relative to the spreading direction in contrast to magmatic segments, and are usually marked by an axial trough rarely more than a kilometre deep. This axial trough may extend 50 km or more. Amagmatic accretionary ridge systems show little volcanic activity and they do not have seismic layer 3, but show mantle peridotite close to the seafloor (Jokat et al., 2003).

Dick et al., (2003), suggested that ultraslow-spreading ridges uniquely dominate amagmatic rifts that expose mantle peridotite directly on the sea floor, with only scattered basalt and gabbro. Amagmatic rifts form a new, fourth class of plate-boundary structure through magmatic rifts, transforms, and subduction zones. For instance an amagmatic segment on the Southwest Indian Ridge (SWIR) (Dick et al., 2003) shows similar characteristics as the segments occuring on the Gakkel Ridge (Michael et al., 2003). Amagmatic segments may also take different orientations to the spreading direction, sometimes forming oblique rifts (Dick et al., 2003; Snow et al., 2001), and they can produce a unique “smooth” seafloor (Cannat et al., 2006).

2.4. Continent - Ocean Transition (COT)

Continent-ocean transition zones occurs at passive margins where there is transition between continent and oceanic crust (Direen et. al., 2007). To understand the processes that take place from continental rifting to formation of oceanic crust, there are some important parameters that need to be understood. These parameters are the width, thickness, and nature of the COT. There are also important factors controlling the magmatic and tectonic processes on these margins. These factors are intraplate

stress distributions, asthenospheric and lithospheric temperature, lithospheric rheology, and the duration and rate of extension (White and McKenzie, 1989; Ruppel, 1995; Manighetti et al., 1997; Courtillot et al., 1999).

There is a coincidence between continental break up and flood basalts (Morgan, 1971). When subareal lava flows observed as seaward dipping reflectors (SDR), that margin is called as volcanic margin (Eldholm et. al., 1987). At the COT zones, wedges of SDRs occur above or seaward of the high velocity lower crust in most volcanic provinces. These reflectors form as the plates move apart, followed by lava extruded on the surface. Later on, as plates move further apart, more layers are extruded. This extra weight, particularly near the extrusion point, causes subsidence and dip of layers as shown in figure 2.4. These sequences are composed of a mixture of volcanic flows, volcaniclastic deposits and non-volcanic sedimentary rocks (Planke et. al., 2000).

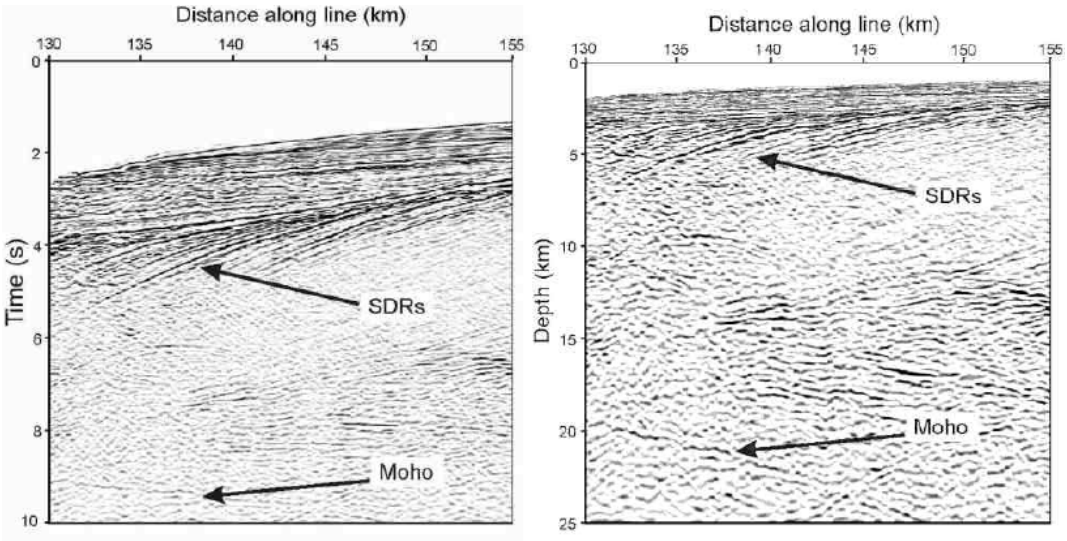

Figure 2. 4. Seaward dipping reflectors (Roberts et al., 1979).

3. GEOLOGICAL BACKGROUND

3.1. Evolution of the Norwegian-Greenland Sea

The ocean that lies between Greenland and Europa is called the Norwegian-Greenland Sea, constrained by the Spitsbergen Zone to the north and by the Greenland-Iceland Ridge to the south. It contains the area north of Iceland, Kolbeinsey Ridge, Aegir Ridge, Mohns ridge and Knipovich Ridge, and Jan Mayen Fracture Zone separates the Kolbeinsey Ridge from the Mohns Ridge (Talwani and Eldholm, 1977) (Figure 3.1).

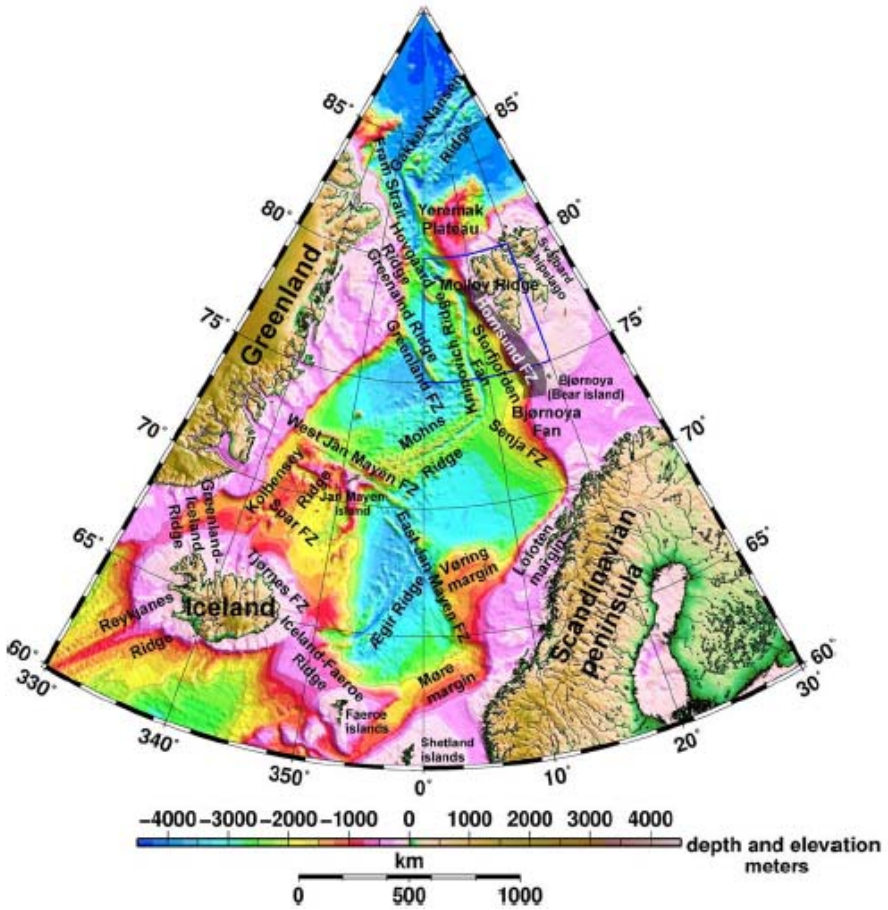

Figure 3. 1. Bathymetric map of the North Atlantic with the most important features on the ocean floor (Kandilarov et.al., 2008).

Before the deep north east Atlantic ocean formed in early Cenozoic time, the North Sea and the Barents Sea were shallow seas, part of a much larger epicontinental sea between the continental masses of Fennoscandia, Svalbard and Greenland (Eldholm

et. al., 1990). The region formed as an epicontinental platform where several marine transgressions and regressions occured. Sea level rised relative to the land and the shoreline moved toward higher ground, resulted in flooding. During the transgression periods, a major part of sediment portions was deposited (Eldholm and Talwani 1977). The intracontinental Barents Sea had several phases of tectonism (Gabrielsen, 1984) after the Caledonian orogenic movements ended in the early Devonian times. There are three major post-Caledonian rifting periods as 1) Late Devonian– mid-Permian (Carboniferous?), 2) Middle Jurassic–Early Cretaceous, and 3) Early Tertiary (Mourad, 2006).

The late Devonian to mid-Permian was characterized by widespread intracratonic rifting, which was followed by the late Caledonian Svalbardian compressive movements. Then a very large post-rift carbonate platform, streching towards present-day Alaska, was developed. Several large-scale basins were formed related to deepseated sutures, as the Nordkapp Basin of the south-western Barents Shelf and the Sverdrup Basin of Arctic Canada. During this period, a series of western highs were tectonically active and show complex formations, the Stappen, Loppa and Sørkapp–Hornsund highs. During the mid-Permian in general, there was decrease in tectonic activity along the western margins (Worsley, 2008).

The western Barents Sea has been tectonically the most active sector during the Mesozoic and Cenozoic times. The older fracture systems forms the basement underlying sediments of the continental shelf of the Barent Sea (Gabrielsen, 1984). These sediments have been effected by the Late Palaezoic to Cenozoic structural development of the Barents Sea. Therefore, Devonian sedimentation has occured in fault-bounded basins which follows the older structural trends. The time period from Triassic to Early Jurassic is accepted as a quiet period, whereas faulting began again in the Mid Jurassic and increased from Late Jurassic to Early Cretaceous. Extreme rates of subsidence occured in the Tromsø Basin and western part of the Bjørnøya Basin during Early Cretaceous. Close to the end of Cretaceous times, reverse faulting and folding together with extensional faulting in some areas became more common (Gabrielsen 1984).

At Early Cenozoic times, the Norwegian-Greenland Sea began to open (Figure 3.2). The opening started at the Paleocene-Eocene transition (anomaly 25/24B time; ca. 57 Ma) which caused formation of the western Barents Sea continental margin (70-80^{0}N) (Faleide et al., 1996). The direction of opening changed its orientation in earliest Oligocene time (anomaly 13; 35 Ma) which also gave rise to further extension and the opening of the northern Greenland Sea as well (Figure 3.2). Changing the direction of spreading caused renewed tectonism and volcanism at the central rifted margin segment (Faleide et al., 1991).

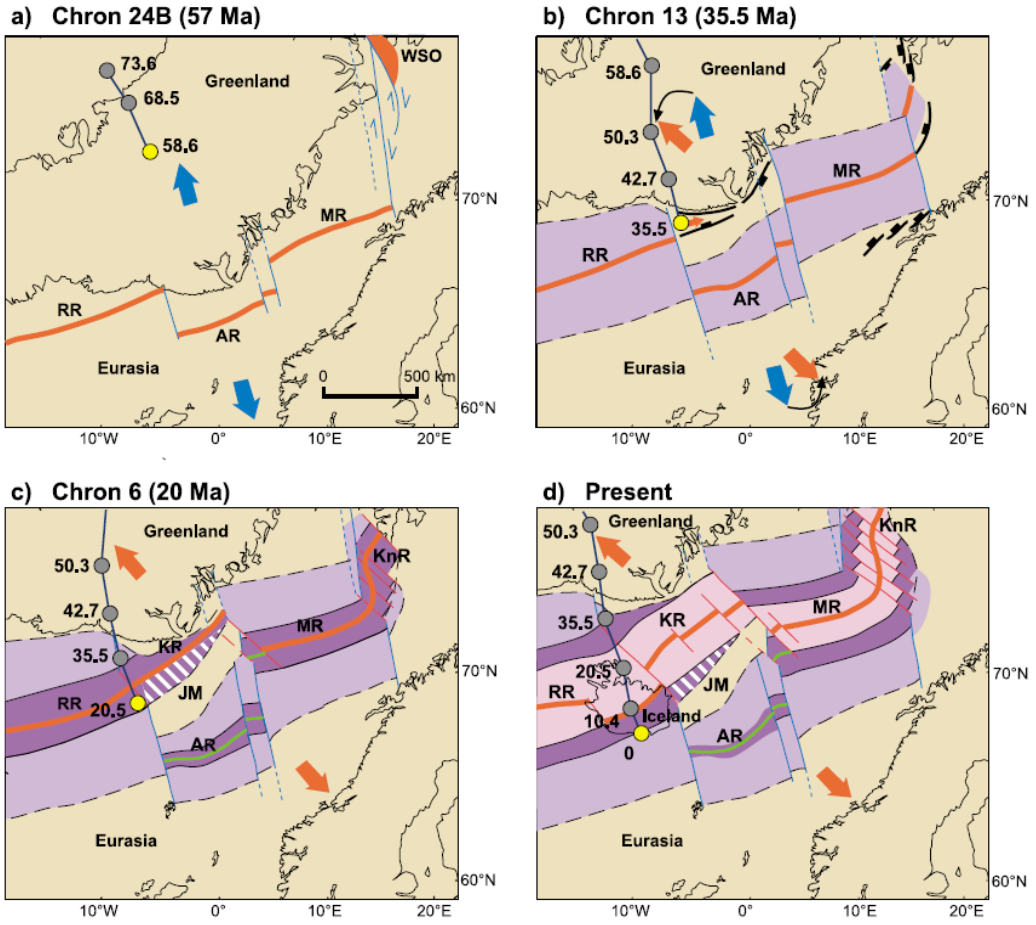

Figure 3. 2. Plate reconstructions. Grey circle represents previous location and yellow circle shows the current reconstruction of the Iceland Plume center (Torsvik et al., 2001). Blue arrows show the spreading direction before 35.5 ma, and orange arrows show spreading direction after 35.5 ma. AR = Aegir Ridge; JM = Jan Mayen; KnR = Knipovich Ridge; KR = Kolbeinsey Ridge; MR = Mohns Ridge; RR = Reykjanes Ridge; WSO = West Spitsbergen Orogeny. From Lundin and Doré (2002).

Since Oligocene times, the oceanic crust has been formed along the Barents Sea margin. The opening was followed by subsidence and accumulation of a thick Late Cenozoic sedimentary wedge fed by erosional products from the Barents Shelf and Svalbard (Eiken and Austegard, 1987). Today the topography of the Barents Sea is effected not only by the underlying bedrock and structural trends. It is also effected by the glacial erosion in late Cenozoic times. It has shallow banks separated by deep troughs. The Bjørnøya and Storfjorden Troughs express the most important morphological features along the western margin. Along the western Svalbard margin there are similar but also smaller troughs. These troughs form the continuation of fjords in Svalbard westwards extending across the relatively narrow shelf. The throughs along the western Svalbard margin are called the Bellsund, Isfjorden and Kongsfjorden Troughs (Faleide et al., 1996).

3.2. The Southwestern Barents Sea margin and adjacent continental shelf

The western Barents Sea and Svalbard continental margin consists of three main structural segments (Figure 3.3).

- southern sheared margin along the Senja Fracture Zone (70-72^0 30`N);
- central rifted complex southwest of Bjørnøya associated with volcanism (72^{0}30`-75^{0}N) ;
- northern sheared and rifted margin along the Hornsund Fault Zone (75-80^{0}N).

The opening direction caused small but distinct angles with the sheared margins at the Hornsund Fault Zone and Senja Fracture Zone, resulting in transform movements with transtensional and transpressional components. Transtension components formed at the Senja Fracture Zone and west of the southern Hornsund Fault Zone connected by a predominantly rifted segment southwest of Bjørnøya. Most likely the Bjørnøya marginal high represents a volcanic edifice at this part of the margin, that is characteristic of the volcanic type of rifted passive margins (Skogseid & Eldholm 1990). The volcanics at Bjørnøya can be seen within a very short distance from landward of the main continental boundary fault. At the beginning, the flows may

have covered a larger area, but later erosion and vertical movements have resulted in the present-day distribution. Later on, this volcanic province experienced reverse faulting in a pullapart tectonic setting (Faleide et. al., 1988). This area received a lot of sediments mainly from the uplifted Stappen High (Fiedler and Faleide, 1996).

The western Barents Sea margin developed as a result of shear movements during the Cenozoic evolution of the Norwegian – Greenland Sea (Talwani and Eldholm, 1977; Reksnes and Vågnes, 1985; Eldholm et al., 1987; Faleide et al., 1991, 1993). Beneath the margin there is large thicknesses of Upper Paleozoic to Cenozoic rocks. The Cenozoic succession can be explained by two main units, 1) pre-glacial strata (G0) and 2) late Cenozoic glacial sediments GI(R7-R5), GII(R5-R1) and GIII(R1-sea floor) (Faleide 1993).

G0 consists of pre-glacial sediments from Early-Mid Tertiary. It is bounded by the oceanic basement and the reflector R7. The GI, GII and GIII are the glacial sequences from Late Cenozoic times, Pliocene- Pleistocene. Reflectors from R7 to R5 forms GI unit. It corresponds with the glacial growth through glaciofluvial sedimentation across the sheld edge. The GII unit contains the reflectors from R5 to R1 reflectors, showing several glacial events (Butt et. al., 2000). There has been a decrease in glacial activity during the deposition of unit GIII (Hjelstuen et. al., 1996) (Figure 3.4).

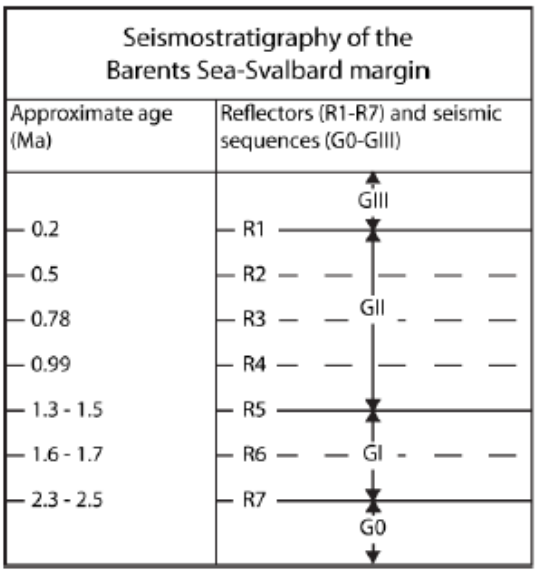

Figure 3. 3. Seismostratigraphy of the western Barents Sea-Svalbard margin with ages, including seven reflectors of four units, Butt et. al., 2000 (Faleide et. al., 1996).

3.3. Knipovich Ridge

The Knipovich Ridge (KR) is an ultra-slow, asymmetrically-spreading ridge which is located in northernmost part of the Mid Atlantic Ridge System. It is the neighboring ridge to the Svalbard continental margin. It is about 500km long and to the south it connects with the Mohns Ridge at 73 50N and it ends to the north at the Molloy Fracture Zone 78 30N (Figure 3.5).

The crustal structure studies at the ultra-slow spreading Knipovich Ridge (KR) have been relatively scarce. KR defined as an ultra-slow spreading ridge, and a typical peculiarity is the diffuse character of the magnetic anomalies (Dick et al., 2003). The suggested causes of the exceptional pattern are thermal blanketing from the thick sedimentary load on the eastern side, a wide zone of magma injection, high heat flow, fragmentation due to axial shifts in the past, slow oblique spreading, or a combination of several of these scenarios (Engen et. al., 2003). Okina et. al.(2002) stated that there is not much known about the crustal structure and nature of the magmatic and amagmatic portions.

In early Oligocene times, the northward development of the Mid Atlantic Ridge was unlocked and the spreading axis propagated into the Spitsbergen Shear Zone. This motion may have caused the Knipovich Ridge to migrate eastwards. Talwani & Eldhom (1977) stated that this eastwards migration can be a reason for poorly developed magnetic anomalies (Figure 3.5). The poorly developed magnetic anomaly pattern in the oceanic crust makes it impossible to determine the age and the rate of spreading from the time scale of magnetic anomalies.

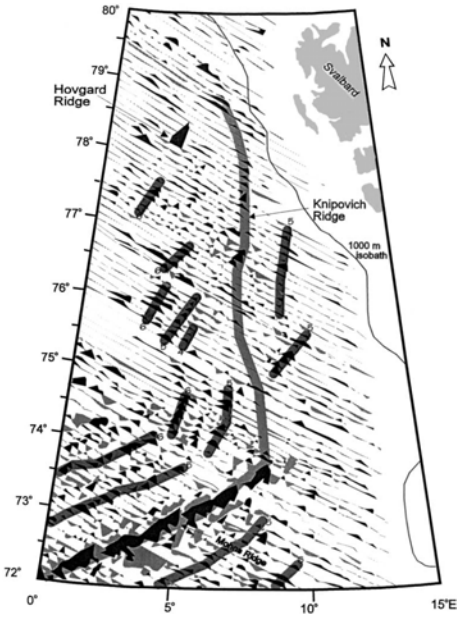

Figure 3. 4. Magnetic anomalies along the Knipovich Ridge. The Knipovich Ridge shown as grey line and the magnetic anomalies as black lines (Crane et al., 2001).

There is an asymmetry in the spreading rate, being 7mm/year to the west and 1 mm/year to the east. This means that the North American plate is moving faster than the Eurasian plate (Kandilarov, 2010).

The ridge has several segments which are cut by axial highs which rise from 600m to more than 1,100m above the rift valley. The axis of the ridge reaches a maximum depth of approximately 3,700m. The axial highs are also volcanically active highs which are responsible for the formation of the seamount chains. These chains and spreading have the same direction (Crane et al., 2001). In addition to these, the axial- and off-axial highs follow highly oblique strike-slip faults. These are considered as

"weak zones" inherited from the evolution of the ancient Spitsbergen Shear Zone (Ljones et al, 2004) (Figure 3.6).

There is a contrast between the northern and southern part of the Knipovich Ridge. The shape of the valley is more ''V'' shaped in the south and ''U'' shaped in the north (Crane et al. 2001a; Engen et al. 2003). Crane et al. (2001a) and Crane (1991), observed 1st to 4th order segmentation along the ridge. 1st order segmentation is seen along the entire rift valley whereas bathymetric highs more than 500m above the adjacent topography shows the 2nd order segmentation, and 200-500m above shows the 3rd order segmentation. 4th order segments are defined by small scale axial shape and depth variations.

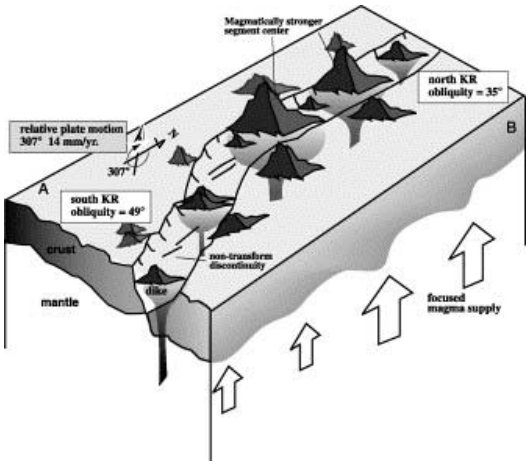

Figure 3. 5. Picture shows the difference between the north and south Knipovich Ridge (Okino, 2002).

The mean axial depth does not change along the Knipovich Ridge. The effect of the Iceland hotspot can be disregardable (Schilling et. al., 1998), and there are no transform faults or large offsets effects on major along-axis changes in lithospheric thickness. The studies have shown no difference between the southern and northern sections of the ridge in the meaning of large-scale thermal structure. But, in contrast to this, there are differences of the obliquity. It suddenly changes from 35° north of 75°50′N to 49° south of that point. For that reason Okino et al. (2002), suggested to compare the northern and southern Knipovich Ridge to see the effect of obliquity on crustal accretion. The southern part of Knipovich Ridge have low relief segment

centers due to high obliquity, low effective spreading rates, less adiabatic melting, and low melting supply. The surface volcanoes fed by the dikes interfere the oceanic crust perpendicular to plate motion. For that reason, the horizontal extention of dikes is limited in this highly oblique rift, which results in smaller-scale bathymetric highs (Okino et al., 2002).

Engen et al. (2003) and Crane et al. (2001a), made an interesting observation for the whole Knipovich Ridge area. They discovered that the western flank is more elevated than the eastern flank. The reason for this can be explained by the substantial amounts of sediments from the Barents Sea shelf and the Svalbard archipelago into the area, which have been effectively dammed by the ridge. For that reason, a large mass of sediments has accumulated east of the ridge whereas almost no sediments have been deposited west of the ridge. This heavy load caused the eastern side of the ridge to subside several hundred meters relative to its western part (Engen et al. 2003; Crane et al. 2001a; Faleide et al. 1996; Fiedler and Faleide 1996; Hjelstuen et al. 1996).

3.4. Bjørnøya Fan

The Bjørnøya Fan is a sedimentary wedge, extending over both oceanic and continental crust. It consists of up to 3-4km of Late Cenozic sedimentary deposits. The constructuion of this fan is as a result of the glaciations at the northern hemisphere. The calculations from the hinterland erosion rates, based on the volume of the sediment wedges, show that during the last 2.5 million years there may have been 1000-1500m of erosion (Figure 3.7) (Vorren et al., 1991; Eidvin et al., 1993; Hjelstuen et al., 1996; Fiedler and Faleide, 1996).

Fiedler and Faleide, 1996, suggested that the Bjørnøya Fan is a major sediment depocenter which contains 70% of the sediment in the entire Lofoten-Basin. The accumulation of sediments are comparable with the sediments accumulation in the Mississippi and Amazon fans since Late Pliocene and Late Miocene. However, since both Mississippi and Amazon fans covers much more larger area than Bear Island Fan, Solheim et. al., 1998, suggested that the Bear Island Fan have much more effcient erosion.

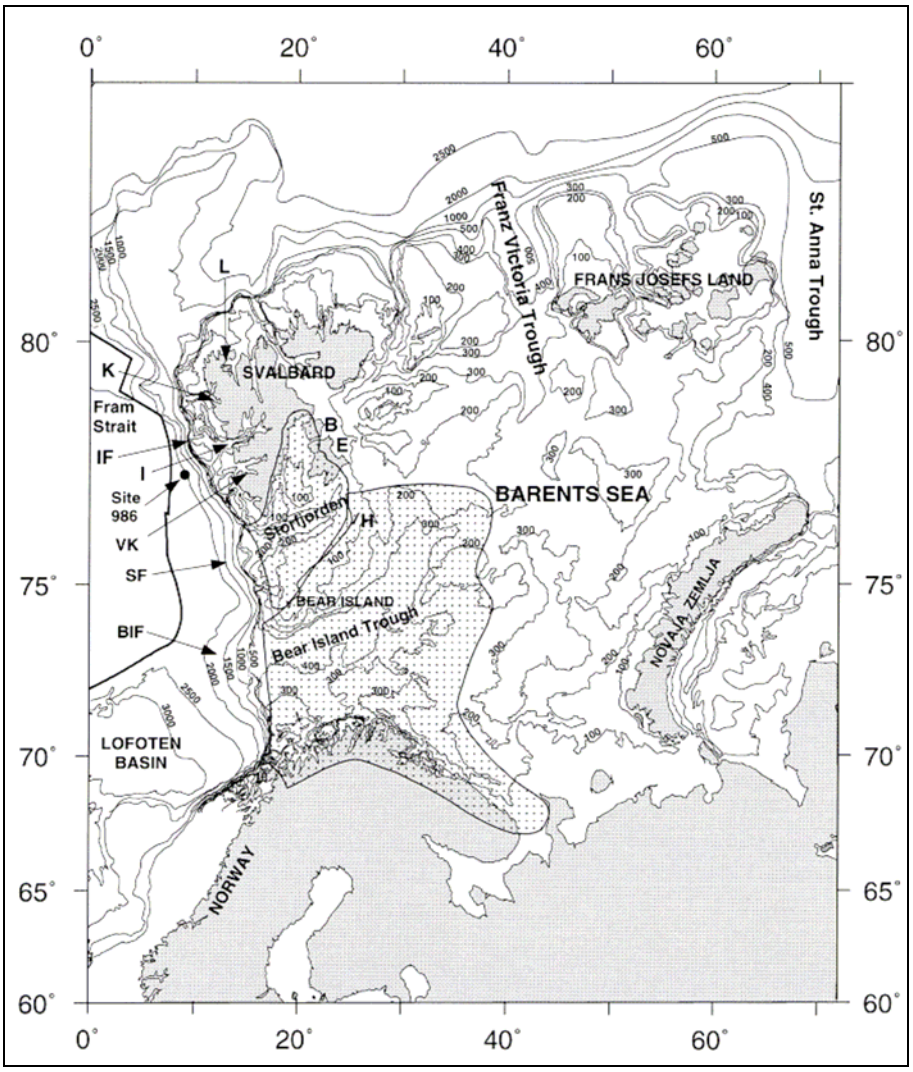

Figure 3.7. Map of the Barents Sea and Svalbard showing drainage areas of the Storfjorden and Bear Island Fans. L=Liefdefjorden; K=Kongsfjorden; I=Isfjorden; VK=Van Keulenfjorden; IF=Isfjorden Fan; SF=Storfjorden Fan; BIF=Bear Island Fan; B=Barentsøya; E=Edgeøya; H=Hopen (Solheim et. Al., 1998).

4. DATA ACQUISITION and PROCESSING

4.1. OBS Data Acquisition

The survey was carried out in 2008 from the Bear Island and westwards across the Knipovich Ridge, by using R/V Håkon Mosby of the University of Bergen. Cooperating institutes were Hokkaido University (Japan), IFM-GEOMAR Kiel (Germany) and University of Warsaw.

Two seismic profiles were acquired on the eastern part of the Knipovich Ridge. Figure 4.1 shows the position of the profiles. BIS-Profile, (Bear Island South), starts from 72^0 6'50''N, 9^0 36'00''E and finishes 74^0 27'36''N, 19^0 15'47''E. BIN-Profile, (Bear Island North), starts from 74^0 56'51''N, 7^0 37'8.04''E which is west of Kipovich Ridge and finishes northwest of Bear Island 74^0 32'32.99''N, 18^0 29'13.1''E.

This thesis focuses on the BIS-profile, along which a total number of fifteen three-component OBS were deployed. The seismic source used for this survey consists of an array with four air guns and TNT shots. The volume of each air gun was 1200 m^3 so one array had a volume of 4800 m^3 (Kandilarov and Mjelde, 2008). The shots were fired every 200 m and triggered by navigational computer. Totally 1914 airgun shots were applied with distance interval of 200 m which corresponds to one minute time interval. Depth of the airguns was approximately 10 m. Totally 104 TNT shots (25 kg of TNT each) were applied by R/V Horyzont II along the northeastern part of the profile, from the distance of 176.4 km to 385.5 km. The average distance interval was 2 km and the depth of TNT explosions was approximately 30 m (Czuba et. al., 2011).

The seismic stations were equipped with Japanese ocean bottom seismometers. Two of the stations did not record seismic data at all (OBS 1 and OBS 11) and OBS 6 started recording after the last airgun shot was fired. So, this station only recorded some of the TNT shots. The positions of the instruments are given in Figure 4.1. The seismometers used in this survey are three component OBS which includes two horizontal and one vertical geophone.

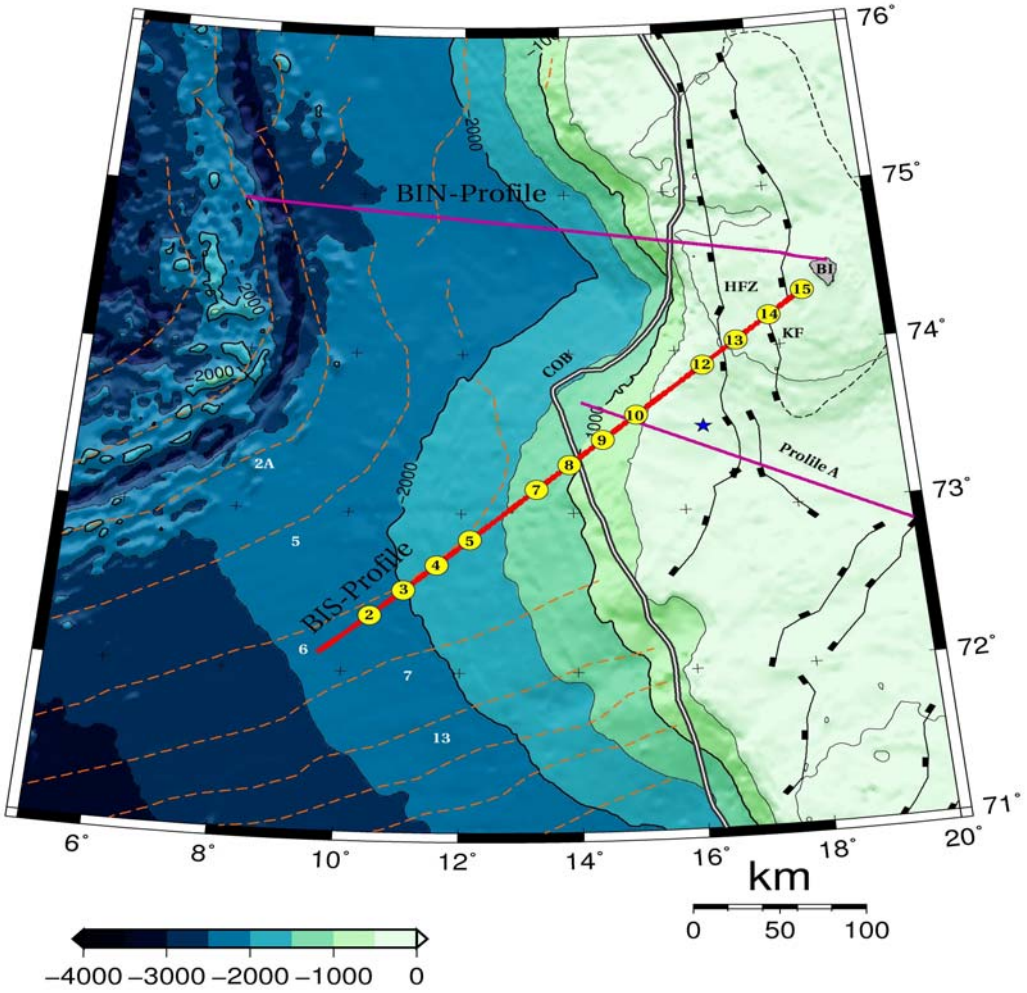

Figure 4. 1. Map of the study area with nearby OBS survey lines and with COB (white line), most important faults (dashed lines) and other elements. On BIS-Profile positions of OBSs are shown. BI=Bear Island; BIN= Bear Island North seismic line; BIS= Bear Island South seismic line; COB= Continent-ocean boundary; HFZ= Hornsund Fault Zone; KR= Knipovich Ridge; MR= Mohns Ridge; SH= Stappen High; Star represents Vestbakken Volcanic Province. Locations and extent of structural elements from Ritzmann and Faleide (2007). COB from Breivik et. al,1999, magnetic anomalies from Engen et. al., 2008. Profile A was taken from Clart et. al., 2011.

4.2. OBS Processing

For processing, the standard OBS data processing in Seismic Unix was applied. This application has four steps as; velocity reduction, bandpass filtering, automatic gain control, and deconvolution.

On the seismograms, we are interested in the areas with arrivals. In order to enhance these areas, a velocity reduction step was used. This is done by changing the time axis into the $time - \frac{offset}{v_{red}}$. v_{red} represents the reduction velocity. The P-wave velocity in the upper mantle has the highest velocity in such refraction studies. Therefore, the velocity reduction for this thesis was chosen as 8km/sec, which makes the arrivals from the upper mantle to appear horizontally on the seismograms. Slower arrivals are seen as dipping arrivals. For the comparison between raw data and velocity reduced data, see figure 4.2.

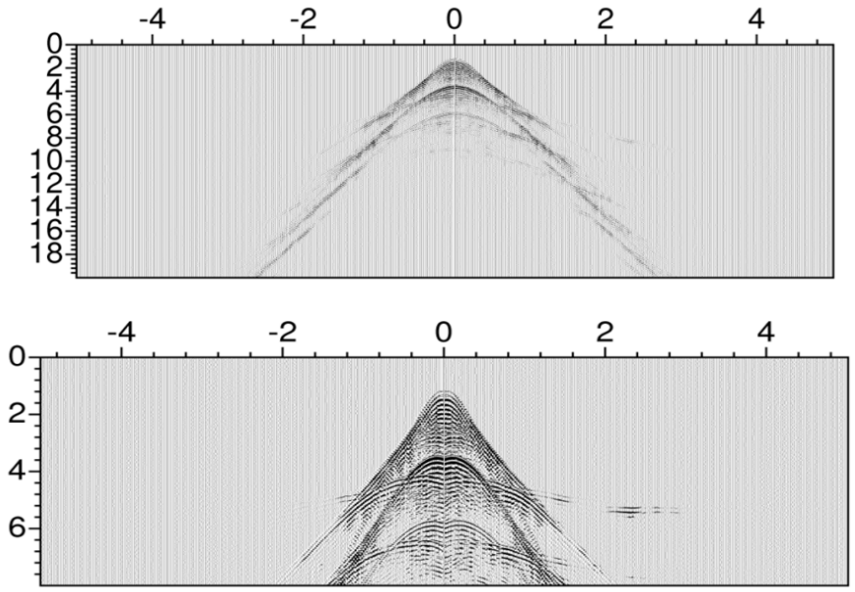

Figure 4. 2. The figure above shows the raw data from OBS 5. Below: the seismogram of OBS 5 after velocity reduction 8 km/s applied.

For OBS processing, after a velocity reduction of 8km/s, bandpass filtering, AGC and deconvolution was used respectively. The ramps of the band-pass filtering was at 2-4Hz and 15-20Hz, and the automatic gain control (AGC) used a 3 seconds window. When the signal and noise have different frequencies, bandpass filters are used to remove the noise from the data. With defined high and low frequencies on the bandpass filter, it cuts the data and noise under and above these frequencies. In this way noise will be attenuated in the data, but the random noise and the noise with the same frequency as the signal will still exist in the data (Figure 4.3).

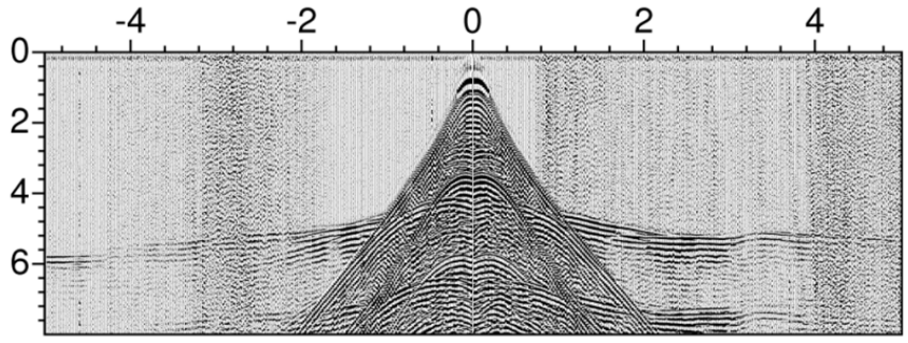

Figure 4. 3. Figure shows the seismogram from OBS 5 after applying band-pass filter.

The working steps for Automatic Gain Control (AGC) is finding the mean amplitudes in a given time window, and multiplying the interval with the number that raises the mean to a predetermined value. AGC decreases the amplitudes of strong arrivals. In contrast, it causes increase in the amplitude of later arrivals and weaker events. This results in increasing late low amplitude arrivals (Figure 4.4).

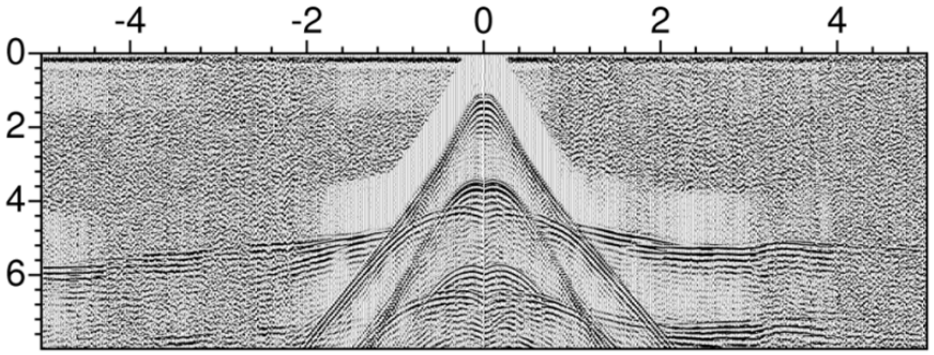

Figure 4. 4. Figure shows the seismogram from OBS 5 after applied AGC of 3sec.

Predictive deconvolution has been applied to all seismograms. The process causes decrease in ringing which may mask later arrivals. Sometimes it shows seismic phases that are not easily seen on the original seismograms (Figure 4.5).

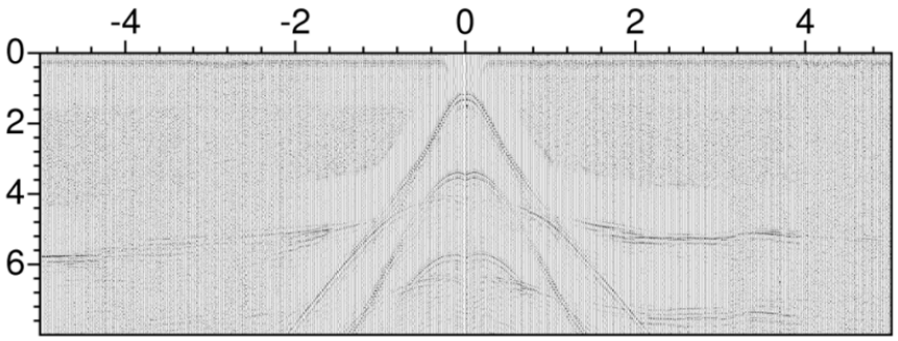

Figure 4. 5. The seismogram from OBS 5 after applied deconvolution.

5. MODELING PROCEDURE

5.1. P-Wave Modeling

GeoGraphix software by Landmark was used to interpret the data from the vertical OBS components. The interpretation was done acknowledging that hyperbolic curves in the seismograms are reflections and refracted waves appear as straight lines. Low velocity causes arrivals to appear with steep dips on the seismograms. These arrivals represent refractions from shallower layers (Figure 5.1).

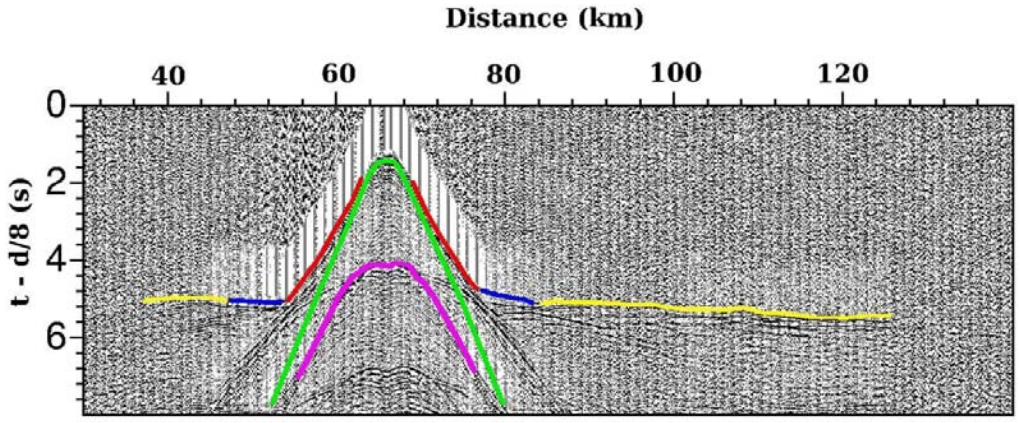

Figure 5. 1. The four phases picked in this thesis are shown on this figure from OBS3. The direct wave (green) has a characteristic hyperbolic shape. The refracted wave from the sediments (red) shows a relatively low apparent velocity (steep dip). The direct wave from oceanic layer 2 (blue). The deeper arrivals (yellow) close to 8 km/s (almost horizontal). The first waterlayer multiple is marked in purple.

After interpretation, a final velocity model was constructed using a layer-stripping way. It is important to model one layer at a time, as discussed by Zelt (1999). After the structure of the velocity is determined, then the next layer is modeled. This procedure was followed during the entire modeling, until to the deepest layer was modeled.

The arrivals were interpreted in four categories. These are; refracted waves from the sediments, refracted waves from the upper crystalline crust, refracted waves from deeper interfaces, and reflections from a few OBSs. This interpretation was done regarding to the shape of the arrival, travel time, and dip (apparent velocity). The

uncertainity values of the picks were estimated at 50ms for the sediments, 75ms for the upper crystalline crust, and 100ms for arrivals from the lower crust and mantle.

For the modeling first the interpreted arrivals were transfered to Rayinvr, where the interfaces are seen as nodes, depth and velocity nodes, interconnected through the profile. Each layer have velocity nodes which contains information about the P-wave velocity at the top and bottom of the layer (Figure 5.2). There is a linear interpolation between the velocity nodes, cause velocity gradients possible both laterally and vertically. The modeling cycle is performed in forward steps, in which the model parameters for the given layer are varied and changed until a resonable fit between the modeled and observed travel time data is achieved. For areas which have complex geology, extra velocity nodes are added to the model. Also the depths of the nodes are seen along the profile (Figure 5.3).

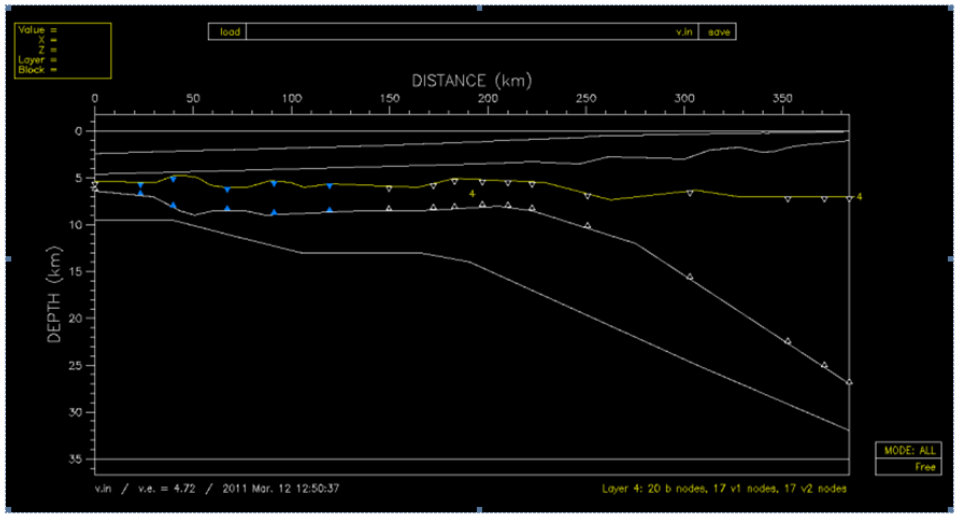

Figure 5. 2. Figure shows the velocity nodes for interface 4, taken from the plotted velocity model, vmed. Having one velocity node at the top of the layer and one at the bottom allows for a velocity gradient within the layer.

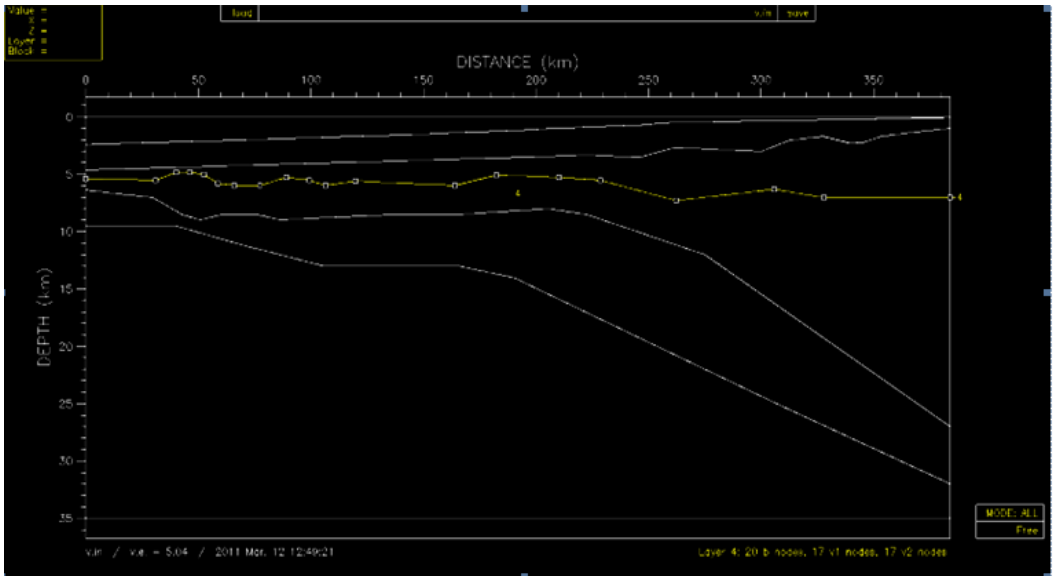

Figure 5. 3. Depth nodes given in the ploted velocity model, vmed, for layer four.

Rayinvr program traces rays through the model, and calculates how well the calculated arrivals fit to the interpreted picks. It shows the calculated rays plotted over the picks (Figure 5.4) which provide the user to see how the model can be changed in order to achieve a better fit. Figure 5.4 displays the path of the rays through the subsurface on top and the lower plot represents how the calculated rays (thin, black lines) fit the picks (short, colored, vertical lines). The size of the vertical lines shows the uncertainity. The bigger the vertical line the higher the uncertainity value. This figure shows a good fit for all layers. The refraftion from sediments are blue picks, the oceanic basement is yellow picks, oceanic layer 3 is purple,the calculated arrival from the Moho is brown colour. The other blue color is the multiple from water layer.

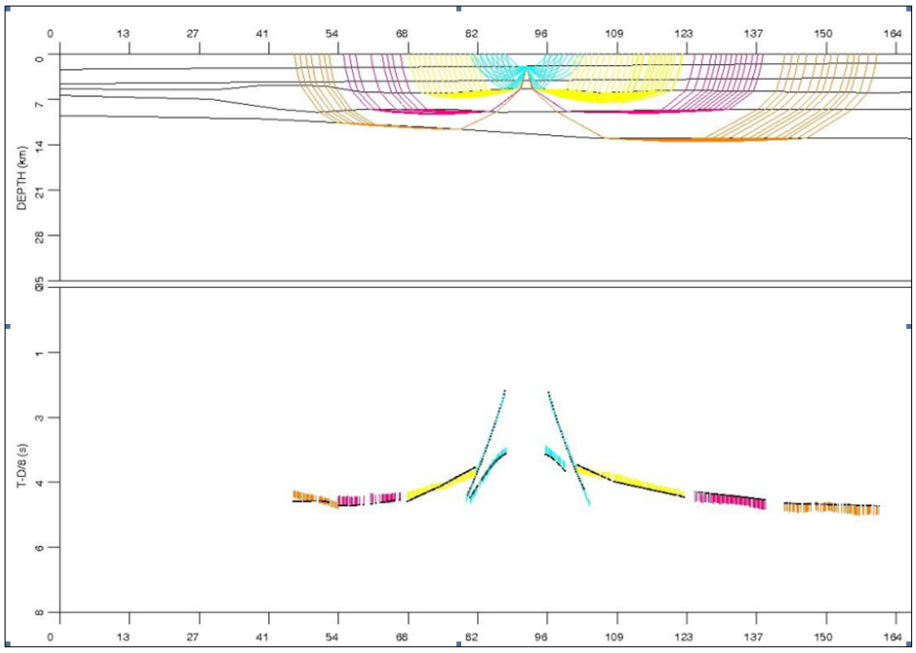

Figure 5.4. Traced rays for OBS 4.

5.2. Uncertainties

By using forward modeling of seismic traveltimes, one should not expect to obtain unique solutions for the final model (Zelt, 1999). The quality of the model depends on many factors such as; OBS data quality, the quality of interpretation of the data and the ray coverage.

The X^2(chi-squared) value shows the fit between the calculated rays and the observed picks in relation to the pick uncertainty (Zelt and Forsyth, 1994). T_0 is the observed arrival time, T_C is the calculated arrival time, U_i is the uncertainty and n is the number of picks. If X^2 is around one, there is an acceptable fit between the calculated and the observed data for the given data uncertainty. Lower values indicate an over-parameterized model (Zelt, 1999).

$$X^2 = \frac{1}{n}\sum_{i=1}^{n}\left(\frac{T_{0_i} - T_{c_i}}{U_i}\right)^2$$

Root mean square (RMS) time values are also calculated with the formula below, in addition to X^2 values. The parameters are the same as the formula for X^2. The RMS time reveals the misfit between calculated and picked arrivals in seconds, the RMS misfit is easy to visualize.

$$T_{rms} = \sqrt{\frac{\sum \left(T_{0_i} - T_{0_c} \right)^2}{n}}$$

X^2 and RMS values for the P-Wave model is presented in table 1.1.

Layer	Wave Type	Number of picks	RMS	X^2
Layer 1	Diving wave	848	0.057	1.285
Layer 2	Diving wave	445	0.082	1.019
Layer 3	Diving wave	1410	0.099	1.295
Layer 4	Diving wave	1110	0.129	1.747
Layer 5	Diving wave	1002	0.140	1.889
Layer 3	Reflected wave	249	0.079	1.121

In order to see where the model is more and less determined Ray hit density map was produced. In this way, it can be seen which parts of the model has good and bad ray coverage (Figure 5.5). The areas that have more than 1000 ray hits, have black colour.

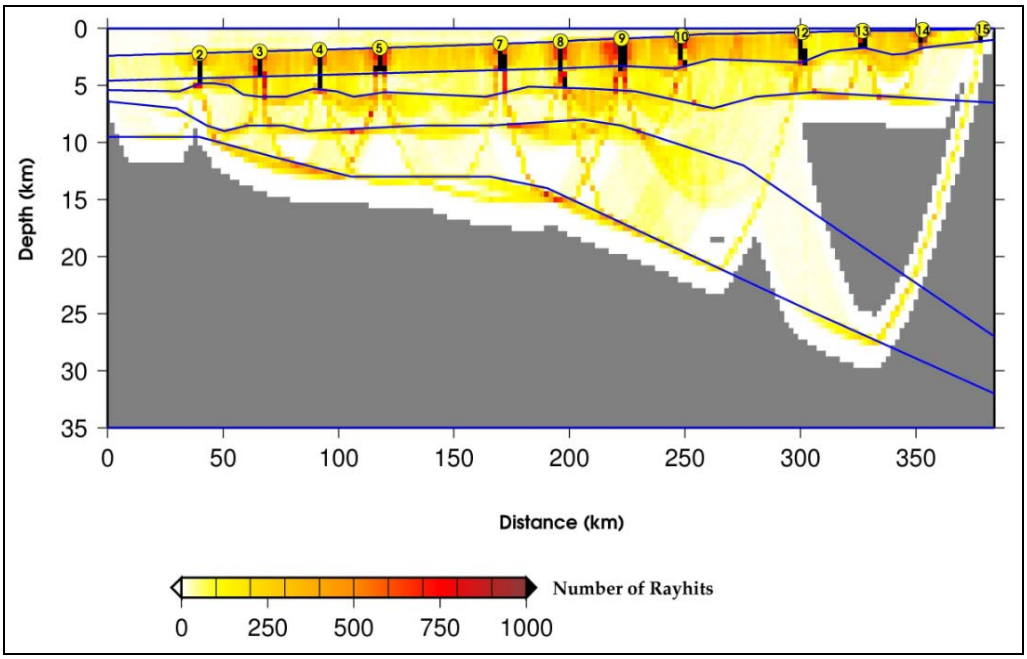

Figure 5. 5. Ray hit map, shows the ray coverage.

6. RESULTS

6.1. Velocity Model

After successive trials, the 2-D velocity model for sediments, crystalline crust and crust–mantle transition was formed (Figure 6.1). According to the model, the whole area can be divided into three parts as oceanic crust, 0 – 190 km distance, continental oceanic transition zone, 190 - 220km, and continental crust, 220 - 384km.

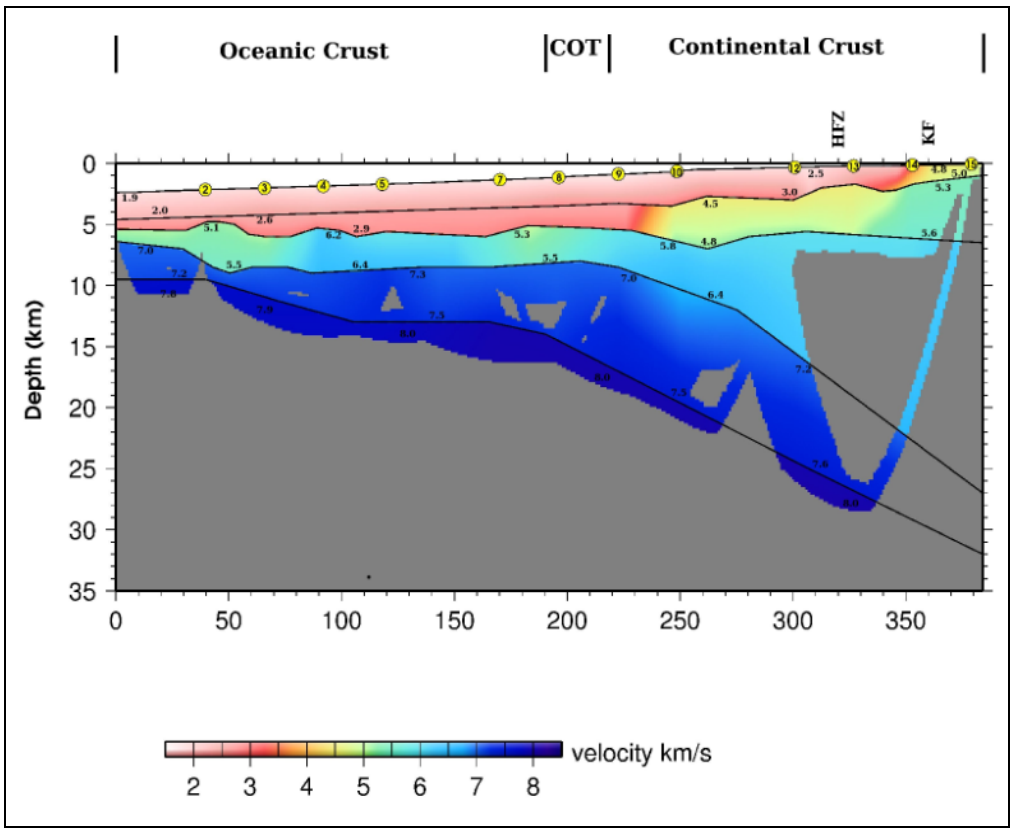

Figure 6. 1. P-wave model of the BIS-Profile.

Refraction seismic showed that the area has seismic velocities typical for oceanic crust until eastward of OBS 7 at about 180 km distance along the profile. OBS 8 and OBS 9, together with eastern part of OBS 7 showed very complex structures, which are seen between 190 km and 240 km offsets along the profile. The location and details regarding to these structures were given at the dicussion part.

From 220 km to the end of the profile, the seismic velocities are typical of continental crust. The effects of the Vestbakken Volcanic Province cause increase in higher velocity values at the second layer from approximately 240 km to the end of the profile.

The Moho depth is from 9,5 km to 14 km under the oceanic crust, whereas it is 15km to 32 km under the continental crust.

6.1.1. The Oceanic Basin

In this study, at the oceanic crust part of the profile sediments and both oceanic layer 2 and oceanic layer 3 are seen. However, no evidence was found for sub-layers 2A, 2B, 2C and 3A, 3B.

Two sedimentary layers were found at the oceanic part. Low velocity values from 1.9-2.0 km/s were found at 2 km thick sedimentary layer 1 and sedimantery layer 2 has 1 – 3 km thickness and has velocities of 2.6 – 2.9 km/s.

The thickness of oceanic layer 2 is variable along the profile. From 0-30 km distance, southwestern end of the profile, the thickness increases gradually from 1,5km to 2km. From 30 km to 60 km, there is decrease in the thickness of the oceanic layer 2. From 60 km to the end of oceanic part at around 190 km, the thickness is about 3 km with some variations. The significance of this shallow structuring is unknown because constraints from multichannel seismic data was not used in this thesis.

The velocity values at oceanic layer 2 increases gradually from 5.1km/s to 5.5km/s from 0 km to 70 km. Between 80 km and 160 km, the velocities are around to 6.2 km/s, which decreases to around 5.3km/s near the COTZ.

The depth to the top of oceanic layer 3 is gradually increasing from 6km to 8,5km between 0 km and 50 km distance along the profile and it remains the same with some small changes until the transition zone.

The velocity of oceanic layer 3 shows very small or close to no changes through the entire profile. The best fit for oceanic layer 3 was obtained for a velocity of 7.0 km/s in the top, and a velocity of 7.2 km/s at the bottom, in the range 0-100 km. Between 100 km and the COT a velocity of 7.5 km/s was found near the base of layer 3.

6.1.2. The continent-ocean transition zone

Since volcanic extrusives covered most of the underlying structures, the transition from ocean to continental crust is not very clear. From the P-Wave model, the COT is located between 190 and 220km, where the oceanic layer 3 terminates against continental crust around 215 km. The seismogram image from OBS 9 shows a clear difference between the west and east side (Figure A.7). The western side shows arrivals similar to the other arrivals on the oceanic crust, whereas the arrivals on the eastern side show that higher velocities must be located much shallower.

6.1.3. The Continental Basin

As it was for the oceanic part, two sedimentary layers were found at this part of the profile. The first sedimentary layer shows almost the same properties as for the oceanic part, 2 km in thickness with velocities of 1.9 – 2.0 km/s, until approximately 320 km distance where the Hornsund Fault Zone (HFZ) is located on the profile. HFZ is located based on the earlier studies. The velocity of the sediments below seabed is 2.5 km/s at HFZ area. The closer to the land, the higher velocities were seen along the profile. From 350 km to the end of the profile, there has been observed high velocities around 4.5 km/s (Figure 6.1). In addition to HFZ, there is one more fault zone named Knølegga Fault along BIS-Profile. This fault was seen on the seismogram of OBSs 14 and 15. The apparent velocities on these OBSs are relatively close to 6 km/s when propagating eastwards from 360 km, where the Knølegga Fault is expected to be located (Gabrielsen et al., 1990) (Figure 4.1).

The second sedimentary layer at the continental part of the profile has higher velocities from 4.5 to 4.8 km/s on top and from 5.3 to 5.6 km/s at the bottom. From 2 km depth at 350 km to 6.5 km depth at 320 km, there observed strong discontinuity in velocity, where the Hornsund Fault Zone is located (Gabrielsen et al., 1990), and the

discontinuity in velocity can be explained by the appereance of this fault zone (see figure 4.1). In addition to fault zones, by taking Vestbakken Volcanic Province into account, the refracted arrivals from the upper sedimentary section were seen from OBS 10 to the eastern end of the profile. The magmatic intrusives may show velocities in the 6.5 km/s range.

Below the uppermost layers, two layers were found which form the crystalline complex of the continental crust with the velocities of 5.8 – 6.4 km/s and 7.2 – 7.6 km/s. The thickness of upper crust increases gradually from 270 km distance to the end of the profile. The depth is around 6 km from 270km distance to the eastern end, while the thickness changes from 4 km to 20 km over the same distance range. The depth of the lower crust increases linearly from COTZ to the end of the profile, where it reaches to depth of 32 km. The velocity value at the bottom of the layer is 7.2 km /s after the transition zone and it incrases to 7.6 km/s at the end of the profile.

6.1.4. The Upper Mantle

The depth of Moho east of 260 km is entirely based on earlier studies (Czuba et al., 2010; Ebbing et al., 2007; Ritzmann et al., 2007), since the upper mantle is not sampled except OBSs 14 and 15, beneath the continental part of the profile. For OBS 15, moho refraction was modelled (Figure 6.1). In addition, an upper mantle refraction has been seen at the seismogram image of OBS 14, between 260 km and 300 km distance. The velocity for the top of the mantle is set at 8 km/s, based on the earlier studies. As a result, Moho is linearly deepening from 15 km at 220km of the profile, to about 32 km at the end of the profile.

7. DISCUSSION

7.1. Sedimentary Section

Thick wedges or fans of glacigenic sediments along the North Atlantic continental margin represents an extensive erosion during the Late Cenozoic Ice Age (Solheim et al., 1998). The largest of these fans is the Bjørnøya Fan, which was depositional center for the sediments during Plio-Pleistocene times. The glaciation started around 3.6Ma, followed by the development of a less rigious ice sheet in the Barents Sea in the period 2.4Ma to 1.0Ma. From 1.0Ma repeated ice sheets developed further towards the shelf edge (Knies et. al., 2009).

Shallow drillhole and multichannel seismic data studies by Faleide et al. (1988) suggested that the P-wave velocities at Bjørnøya Fan changes with depth from 1.6 to 2.5 km/s. The sedimentary layer 1 at BIS-Profile has low velocities (1.9km/s) near the seabed on the abyssal plain and at continental slope, which are typical velocities for shallow, unconsolidated sediments (e.g. Breivik et al., 2003). With the investigation of contours and gravitational instabilities, Solheim et. al. (1998) suggested that sediments in this area were deposited as glacigenic debris flows. Therefore, in this thesis, the uppermost sedimentary layer in the model is interpreted as being part of the Plio-Pleistocene glacigenic fan with velocities of 1.9 km/s to 2.0 km/s (Figure 7.1).

At sedimentary layer 1, also observed very high velocities in the seabed (4.8 - 5.0 km/s) from 350 km to the end of the profile. However, it is not typical to have high sedimentary rock velocities (above 4 km/s) just below the seafloor in the continental crust. Having high velocities can be as a result of increased overburden and subsequent consolidation and erosion due to glaciers in the Plio-Pleistocene (e.g. Ottesen et al., 2005). P-wave model shows velocity discontinuity at 350 km, where it is suggested in this thesis that there should be exhisting a fault. Therefore, the Knølegga Fault (KF) was located at 350 km distance at the BIS-Profile (Figure 7.1). Gabrielsen et. al., 1990, suggested that KF have a listric geometry as it is steep on top layer and flattening out until Jurassic at the layer beneath. P-wave model shows this listric structure in this thesis, where observed discontinuties both at sedimentary layer 1 and 2 exists (Figure 6.1). With the interpretation of multichannel seismic (MCS)

data, Faleide et. al. (1988) suggested that Permian/Carboniferous sedimentary rocks outcrop on the seafloor near the northeastern end of the profile. The velocities of these outcrops are slightly above 5.0 km/s, and for that reason this part of sedimentary layer 1 is interpreted as mostly from Permian/Carboniferous times. The location of KF at this thesis is also in accordance with the earlier MCS data interpretation by Faleide et. al. (1988). In addition to KF, there is one more fault zone along the profile, named Hornsund Fault Zone (HFZ). However, this fault zone was not observed as velocity discontinuties in this thesis. The location of HFZ was taken from the earlier studies.

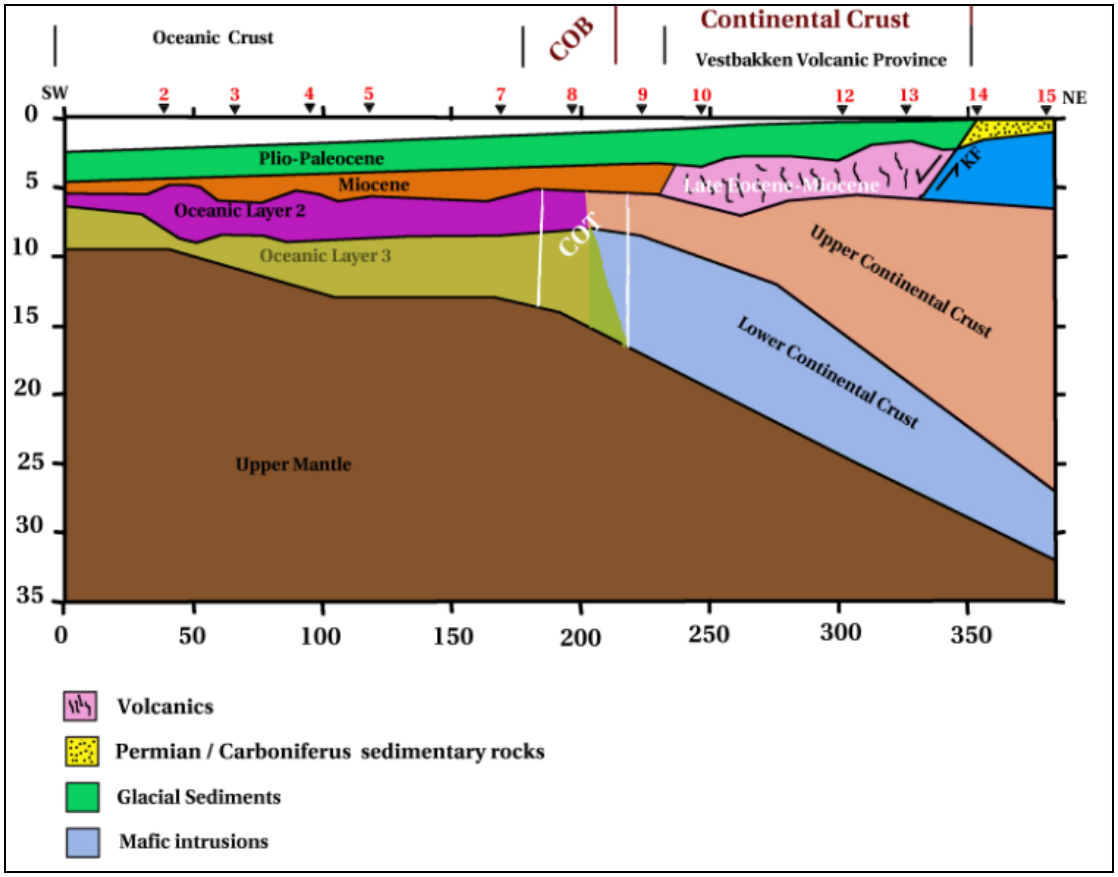

Figure 7. 1. Figure represents the geological model of BIS-Profile

The sedimentary layer 2 in the model, is divided into two geological times. From the southernwest part of the profile until to the COB, it is assumed to be Miocene. From the COB towards east, it is suggested that this area represents late Eocene-Miocene sedimentary rocks (Faleide et al, 1996) (Figure 7.1).

In this thesis it is found that the post-opening sediment thickness at the oceanic crust reaches 5km close to the COB, which correlates well with the results from Hjelstuen et al. (1996).

Sedimentary layer 2 has increasing velocity from 230 km towards the eastern end of the profile. Since the Vestbakken Volcanic Province is located in this part of the profile (Figure 7.1), the increased velocities are probably cause by intrusive and extrusive volcanic rocks. This is also observed in well 7316/5-1 in Vestbakken Volcanic Province where Eocene and older sedimentary rocks are cut by high velocity volcanic intrusions (sills).

7.2. Oceanic Crust Velocities

It is worth mentioning that the oceanic spreading axis is close to western side of the BIS-profile. Between 0 km and 80 km distance the modelling indicates relatively low P-wave velocities in oceanic layer 2 compared to the area further eastwards (Figure 6.1). The P-Wave velocities at this part of the profile are typical for oceanic layer 2, around 4.9 km/s at top of the layer and at the bottom of the layer it is 5.4 km/s, documenting a consistent gradient in this part of oceanic layer 2. These typical velocities in oceanic layer 2 suggests that this layer consists of mature basaltic pillow lavas and feeder dikes.

From 80 km to approximately 180 km distance, there is an increase in the velocity values from 6.0 km/s to 6.2 km/s on the top and from 6.3 km/s to 6.5 km/s at the bottom oceanic layer 2. As Jacobson (1992) suggested, it is common that the seismic velocity increases in oceanic layer 2 with increasing distance from the spreading axis. When there is a decrease in porosity of the extruded basalts due to the filling of cracks by hydrothermally formed minerals, and by closing of microcracks due to increased

sedimentary overburden, then the velocity increases. A small decrease in porosity can cause a large increase in seismic velocity values (Wilkens et al., 1991).

From 0 km to approximately 80 km distance at the southwestern part of the profile oceanic layer 3 has the velocities of 7.0 km/s on top and 7.2 km/s at the bottom, represents gabbroic complex. From 80 km distance the increase in velocities to 7.3 km/s on top and 7.5 km /s can be related to sedimentary overburden.

7.3. Thickness and Depth of Oceanic Crust

The oceanic crust was divided into two parts as northeast and southwest of 100 km. The southwest part of 100 km at BIS-Profile, the oceanic crust is more and less parallel to the Mohns Ridge. Czuba et. al., 2011, suggested that oceanic crust at the part was formed ca 20m.a. P-Wave model for BIS-Profile shows that the thickness of the oceanic crust here is about 4 km, which is normal for ultra slow spreading ridges (Klingelhofer et al. 2000a,b).

When a new portion of an oceanic crustal plate is formed, it will be hot and thermally expanded. As this new portion moves away from the spreading ridge, it will cool and shrink (Sclater et al., 1970). The depth of oceanic crust increases further eastwards, since the location of the spreading ridge is close to the western part of the BIS-Profile.

From 100 km to the northeast-ward, the oceanic crust has been created by the Knipovich Ridge from continental break-up from approximately 35m.a. until 20m.a. Here, the thickness of the magmatic portion of the crust is approximately 8 km. However, as a result of reduced magma generation due to conductive cooling of the lithosphere, the thickness of the oceanic crust generated at ultraslow spreading ridges should be thinner than 6 km (White et al., 1992). So, 8 km thick oceanic layer is thicker than normal (White et al. 1992; Kandilarov et al. 2008). The reason of this thickness is most likely caused by increased magma supply due to the proximity to the Vestbakken Volcanic Province during its most active phase in early Eocene (Faleide et al., 1988). Moreover, Mjelde et al., 2008, suggested the increased magmatism and thereby the increase in the thickness of the crust can be belong to influence from the Icelandic Plume, as it had low activity in this period. Czuba et. al., 2011, interpret the

increased magmatism as a passive response to the (extensional) bending of this southernmost part of the Knipovich Ridge (Figure 7.2).

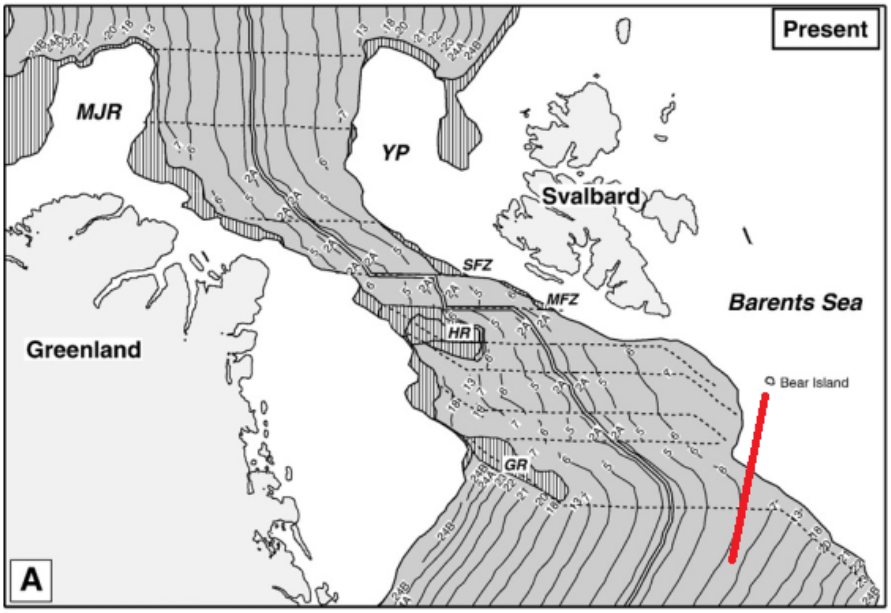

Figure 7.2. Figure shows magnetic seafloor spreading anomalies (bold lines) and BIS-Profile (red line). Note the bending of Knipovich Ridge, (Engen et. al., 2008).

7.4. The continent–ocean-transition (190–220 km)

The oceanic to continental transition zone is observed in a narrow zone, between 190 and 220km, about 30km wide, which may represent the continental shear zone within which a component of extension resulted in stretching of the continental crust (Reksnes and Vågnes, 1985; Eldholm et al., 1987). It is most probable that the crust within this zone consists of thinned continental crust which is intruded and covered by volcanic material mixed with syn-rift sediments.

The modeled oceanic crystalline crust terminates against the continental crust from 215 km to eastwards. Seismogram image for OBS 9 shows clear difference between the east and west sides (Figure A.7). The arrivals at the eastern side show that higher velocities must be located much shallower which shows continental crust characteristics. The arrivals at the western side shows similar characteristics to the other arrivals on the oceanic crust. Since from the P-Wave model the location of COTZ was decided to be located between 190-220km. After observing that oceanic

crust terminates to continental crust around 215 km, the COB is located approximately around 200 km distance along the profile. This location of the COT is in accordance with the position from Breivik et. al, 2007, who located COTZ at about 200km (Figure 7.3).

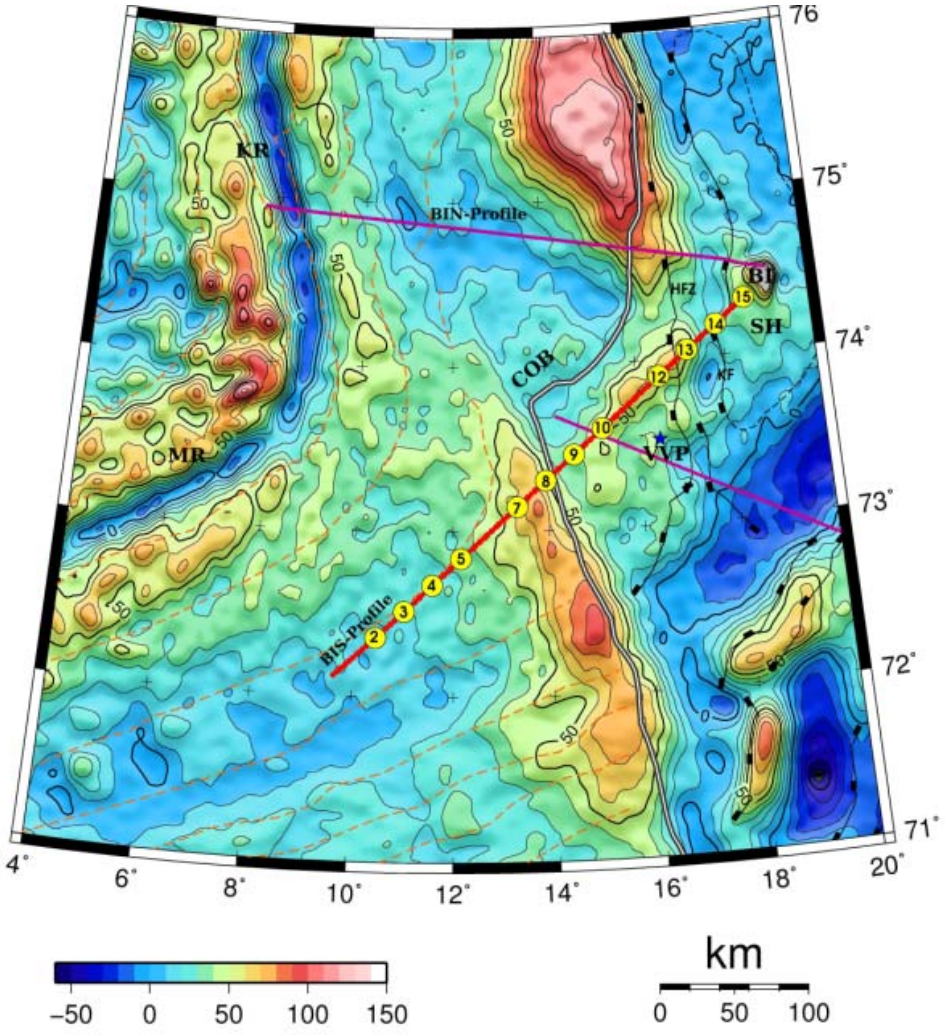

Figure 7. 3. Free air anomalies in the study area. Gray line shows COB from Breivil et. al., 1999. BI= Bear Island; BIN= Bear Island North profile, BIS= Bear Island South profile; COB= Continent-Ocean boundary; KR= Knipovich Ridge; MR= Mohns Ridge; SH= Stappen High; VVP= Vestbakken Volcanic Province.

Faleide et al. (1993) suggested the presence of a basement high, interpreted as volcanic extrusives, protrusions, from around 150 km and 240 km distances along

this profile. Such features are observed on OBSs 7, 8 and 9 (figure 7.4). Please see A.5 for OBS 7 and A.6 for OBS 8.

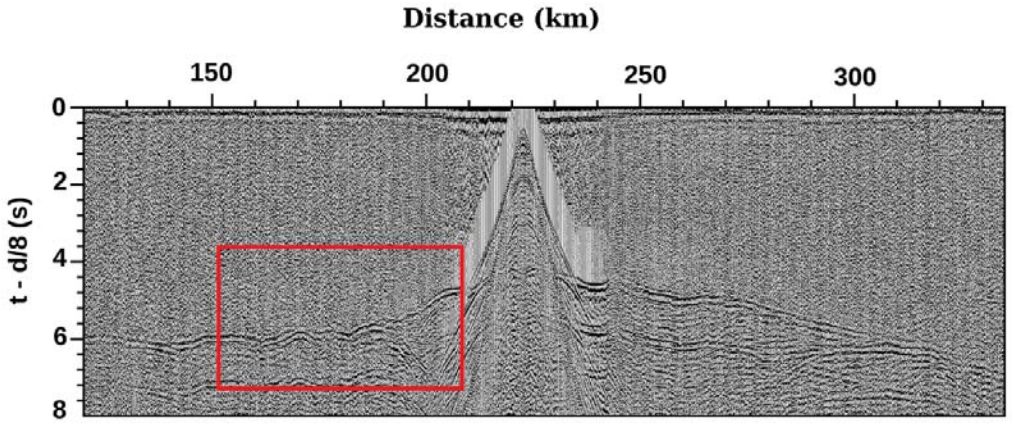

Figure 7. 4. Volcanics observed at OBS 9.

In order to fit to the model, these features caused many trials. Such as; models with a high and narrow basement, models with an increasing P-wave velocity in the oceanic crust, and models with a shallowing of the Moho. But, as it can be seen in figure 7.5, none of them provided a good match. It is suggested that the effects seen in the seismograms result from the magma production at the Vestbakken Volcanic Province.

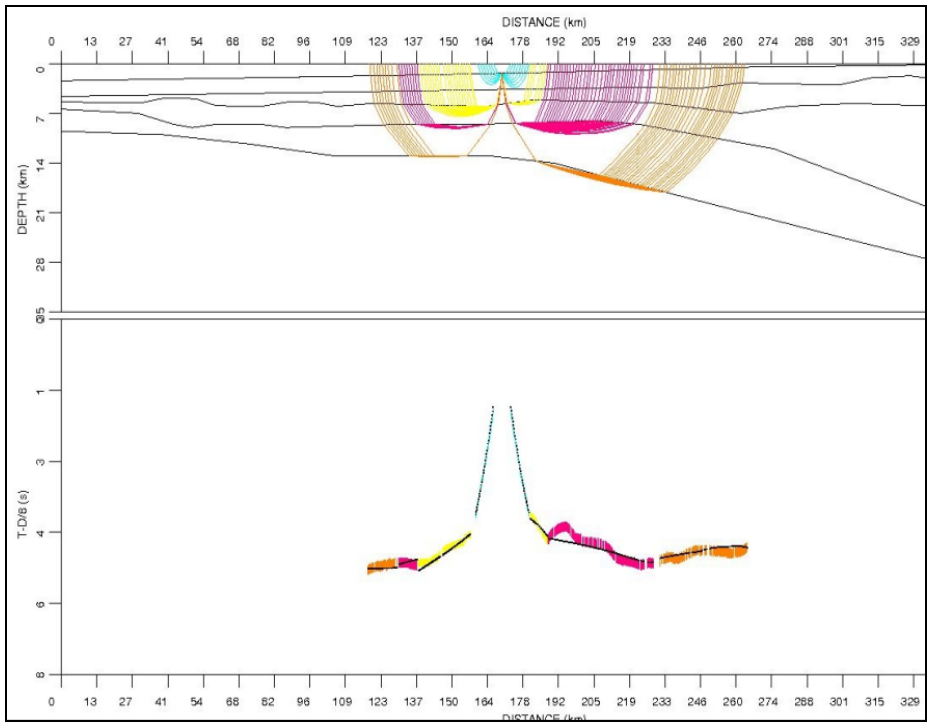

Figure 7. 5. Figure shows modeling of protrusions was challenging.

7.5. Continental Crust

The continental crystalline crust is modelled as two layers. The upper layer has P-wave velocities of 6.2 to 6.4 km/s, which is common for granitic/granodioritic continental crust (e.g. Mjelde et al. 2002a).

The lower crust has velocities of ca 7.5 km/s. In this thesis, the layer is interpreted as a mixture of mafic intrusions and continental crystalline blocks. This interpretation is also similar to the current models applied for the outer mid-Norwegian margin (e.g. Mjelde et al. 2009). White and McKenzie (1989) suggested that higher than normal temperature in the mantle results in higher velocity due to increased Mg content in the melt.

During the Paleocene-Early Eocene phase of rifting there was heat softening at lower crustal levels. The main part of the Vestbakken Volcanic Province was made up of mafic intrusions in the lowermost crust and volcanic activities (Czuba et. al, 2011).

Mjelde et. al. (2009) suggested that the Iceland Plume in the Early Eocene had effect as far north as the Senja Fracture Zone.

8. SUMMARY and CONCLUSIONS

A P-wave velocity model has been constructed from the P-waves in a 384 km long profile. The profile starts from the Bear Island and reaches to oceanic crust which was formed along the Mohns Ridge. The modeled area is divided into three parts as oceanic crust, 0 – 190 km distance, continental oceanic transition zone, 190 – 220 km, and continental crust, 220 – 384 km.

Sedimentary layer 1 has the velocities of 1.9 km/s to 2.0 km/s until 250 km distance along the profile. This part is interpreted as being part of the Plio-Pleistocene glacigenic deposits. Between 250 km and 350 km is interpreted as Miocene – Eocene, since the velocities are from 2.5 km/s to 3.0 km/s. From 350 km to the end of the profile is interpreted as Mezosoic, mainly Cretaceous and velocities at this part are from 4.8 km/s to 5.0 km/s. Under the deposits of sedimentary layer 1, from 250 km, there exists thick layer of volcanics as sedimentary layer 2. These volcanics comes from the Vestbakken Volcanic Province.

Southwestern part of the model represents oceanic crust. Sedimentary layer 2 has the velocites from 2.5 km/s to 3.0 km/s, which is interpreted as Miocene until COB. The thickness of sediments varies from 3 km at the soutwest to 5 km near COB. From 80 to 180 km, oceanic layer 2 is 6 km thick and has the velocities from 6.0 km/s to 6.2 km/s on the top and from 6.3 km/s to 6.5 km/s at the bottom. The increase in velocities is probably as a result of having lower porosities due to age and increased sedimentary overburden.

Northeastern part of the profile represents continental crust, 220 – 384 km. Both the upper and lower crystalline crust are modeled. The upper continental crust gets thicker towards to end of the profile. At 220 km, it is approximately 6 km thick, where as at the end of the profile it reaches to thickness of approximately 20 km.
The location of HFZ was taken from the earlier studies, that it is located at 320 km. The location of COB is in accordance with the earlier studies, which is located approximately 200 km at the profile. The depth to the Moho is 9.5 km around at the southwestern part of the profile, and decreases to 32 km at the northeast part of the profile.

REFERENCES

Artemieva, I.M., 2002. Continental Crust. In: Encyclopedia of Life Support Systems (EOLSS), Developed under the Auspices of the UNESCO, EOLSS Publishers, Oxford, UK [http://www.eolss.net]. Chapter 6.16.3.1.

Auzende, J.M., Bideau, D., Bonatti. E., Cannat, M., Honnorez, J.. Lagabrielle, Y., Malavieille, J., Mammaloukis-Frangoulis, V. and Mtvel, C., 1989a. Direct observation of a section through slow spreading oceanic crust. Nature, 337: 726-729.

Breivik, A.J., Verhoef, J. and Faleide, J.I., 1999. Effect of thermal contrasts on gravity modeling at passive margins: Results from the western Barents Sea. Journal of Geophysical Research, 104: 15293-15312.

Butt, F.A., Elverhøi, A., Solheim, A., and Forsberg, C.F., 2000. Deciphering late Cenozoic development of the western Svalbard margin from ODP Site 986 results. Marine Geology 169 (3–4): 373-390.

Cannat, M., Sauter, D., Mendel, V., Ruellan, E., Okino, K., Escartin, J., Combier, V., and Baala, M., 2006. Modes of seafloor generation at a melt-poor ultraslow-spreading ridge. Geology, 34: 605-608

Courtillot, C. Jaupart, I. Manighetti, P. Tapponier and Besse J., 1999. Earth Planet. Sci. Lett. 166-177.

Clark S. A., Faleide J. I, Hauser J., Ritzmann O., Mjelde R., Ebbing J., Thybo H., Flüh E., 2011. Markov Chain Monte Carlo velocity inversion of seismic reflection/refraction traveltime data for crustal structure of the southwest Barents Sea. Journal of Geophysical Research, submitted.

Crane, K., Sundvor, E., Buck, R. and Martinez, F., 1991. Rifting in the northern Norwegian-Greenland Sea: Thermal tests of asymmetric spreading. Journal of Geophysical Research, 96(B9): 14529-14550.

Crane, K., Doss, H., Vogt, P., Sundvor, E., Cherkashov, G., and Poroshina, I., 2001a. The role of the Spitsbergen shear zone in determining morphology, segmentation and evolution of the Knipovich Ridge. Mar Geophys Res 22:153–205.

Czuba, W., Grad, M., Mjelde, R., Guterch, A., Libak, A., Krüger, F., Murai, Y., and

Schweitzer, J., 2011. Continent-ocean-transition across a rifted shearmargin: off Bear Island, Barents Sea. Geophysical Journal International, 184:541-554.

Dauteuil, O. and Brun, J. P., 1993. Oblique rifting in a slow spreading ridge. Nature, 361: 145−148.

Dick, H.J.B., Lin, J. and Schouten, H., 2003. An ultraslow-spreading class of ocean ridge. Nature, 426(6965): 405-412.

Dimakis P., Braathen, B.I., Faleide, J.I., Elverhøi, A. and Gudlaugsson, S.T., 1998. Cenozoic erosion and the preglacial uplift of the Svalbard–Barents Sea region. Tectonophysics 300: 311–327.

Direen N.G., , Borissova I., Stagg H. M. J. , Colwell J. B. and Symonds P. A., 2007. Nature of the continent–ocean transition zone along the southern Australian continental margin: a comparison of the Naturaliste Plateau, SW Australia, and the central Great Australian Bight sectors. Exploration Geophysics, 32: 252–262.

Ebbing, J., Braitenberg, C., and Wienecke, S., 2007. Insights into the lithospheric structure and tectonic setting of the Barents Sea region from isostatic considerations. Geophysical Journal International, 171: 1390-1430.

Eidvin, T. and Riis, F., 1989. Nye dateringer av de tre vestligste borehullene i Barentshavet. Resultater og konsekvenser for den tertiaare hevingen Norw. Petrol. Direct. Contrib. 27-44 pp.

Eidvin, T., Jansen, E. and Riis, F., 1993. Chronology of Tertiary fan deposits off western Barents Sea: implications for the uplift and erosion history of the Barents Sea shelf. Marine Geology, 112: 109-131.

Eiken, 0. and Austegard, A., 1987. The Tertiary erogenic belt of West-Spitsbergen: seismic expressions of the offshore sedimentary basins. Norsk Geol. Tidsskr., 67: 383-39.

Eldholm,O., Faleide, J.I. and Myhre, A.M., 1987. Continental-ocean transition at the western Barents Sea/Svalbard continental margin. Geology, 15: 1118–1122.

Eldholm, O., Skogseid, J., Sundvor, E. and Myhre, A.M., 1990. The Norwegian Greenland Sea. In: A. Grantz, L. Johnson and J.F. Sweeney (Editors), The Geology of North America. Vol. L, The Arctic Ocean Region. The Geological Society of America, Boulder, CO, pp. 351– 364.

Engen, O., Eldholm, O., Bungum, H., 2003. The Arctic plate boundary. J Geophys Res. 108(B2):2075.

Faleide, J.I., Myhre, A.M., and Eldholm, O., 1988. Early tertiary volcanism at the western Barents Sea margin, in Early Tertiary Volcanism and the Opening of the NE Atlantic, edited by A.C. Morton and L.M. Parson, Geol. Soc. Spec. Publ., 39:135-146

Faleide, J.I., Gudlaugsson, S.T., Eldholm, O., Myhre, A.M., and Jackson, H.R., 1991. Deep seismic transects across the western Barents Sea continental margin. Tectonophysics, 189: 73–89.

Faleide, J.I., Solheim, A., Fiedler, A., Hjelstuen, B.O., Andersen, E.S. and Vanneste, K., 1996. Late Cenozoic evolution of the western Barents Sea-Svalbard continental margin. Global and Planetary Change, 12: 53-74.

Faleide, J.I., Tsikalas, F., Breivik, A.J., Mjelde, R., Ritzmann, O., Engen, Ø., and Eldholm, O., 2008. Structure and evolution of the continental margin off Norway and the Barents Sea. Episodes, 31 (1): 82-91

Fiedler, A. and Faleide, J.l., 1996. Sedimentation along the south-western Barents Sea margin in relation to uplift and erosion of the shelf. Global Planet. Change, 12: 75-93.

Gabrielsen, R. H., 1984. Long-lived fault zones and their influence on the tectonic development of the southwestern Barents Sea. J. Geol. Sot. London, 141: 651-662.

Gabrielsen, R.H., Færseth, R.B., Jensen, L., and Riis, F., 1990. Structural elements of the Norwegian continental shelf: Part 1. The Barents Sea Region. NPD Bull., vol. 6. Nor. Petrol. Dir., Stavanger, Norway.

Gudlaugsson S.T, Faleide, J.I, Johansen, S.E. and Breivik, A.J., 1998. Late Palaeozoic structural development of the southwestern Barents Sea. Marine and Petroleum Geology, 15: 73–102.

Hjelstuen, B.O., Elverhøi, A. and Faleide, J.I., 1996. Cenozoic erosion and sediment yield in the drainage area of the Storfjorden Fan. Global and Planetary Change, 12: 95-117.

Jacobson, R. S., 1992. Impact of crustal evolution on changes of the seismic properties of the uppermost oceanic crust. Rev. Geophys., 30: 23–42.

Jakobsson, M., Cherkis, N.Z., Woodward, J., Macnab, R. and Coakley, B., 2000. New grid of Arctic bathymetry aids scientists and mapmakers. EOS, Trans. AGU, 81(9): 89- 96.

Johansen, S.E., Ostisty, B.K., Birkland, O., Fedorovsky, Y.F., Martirosjan, V.N., Christensen, O.B., Cheredeev, S.I., Ignatenko, E.A. and Margulis, L.S., 1993. Hydrocarbon potential in the Barents Sea region: play distribution and potential. In: T.O. Vorren, E. Bergsager, O.A. Dahl-Stamnes, E. Holter, B. Johansen, E. Lie and T.B. Lund (Editors), Arctic Geology and Petroleum Potential, Vol. 2. NPF Special Publication, Elsevier, Amsterdam, pp. 273-320.

Jokat, W., Ritzmann, O., Schmidt-Aursch, M.C., Drachev, S., Gauger, S., and Snow, J., 2003. Geophysical evidence for reduced melt production on the Arctic ultraslow Gakkel mid-ocean ridge: Nature, 423: 962–965.

Harrison, C.G.A. and Bonatti, E., 1981. The oceanic lithosphere. In: C. Emiliano (Editor), The Sea. Vol. 7. Wiley, New York, pp. 21-48.

Kandilarov, A., Mjelde, R., Okino, K. and Murai, Y., 2008. Crustal structure of the ultra slow spreading Knipovich Ridge, North Atlantic, derived from OBS, MCS and gravity data, along a presumed amagmatic portion of crustal formation. Mar. Geophys. Res., 29: 109–134.

Kearey, P. and Vine, F.J., 1996. Global Tectonics, 2nd edition. Blackwell Publishing, New York, 333 pp.

Klingelhofer, F., Geli, L. and White, R.S., 2000a. Geophysical and geochemical constraints on crustal accretion at the very-slow spreading Mohns Ridge. Geophys. Res. Lett., 27(10): 1547–1550.

Klingelhofer, F., Geli, L., Matias, L., Steinsland, N. and Mohr, J., 2000b. Crustal structure of a super-slow spreading centre: a seismic refraction study of Mohns Ridge, 72.N. Geophys. J. Int., 141: 509–526.

Knies, J., Matthiessen, J., Vogt, C., Laberg, J.S., Hjelstuen, B.O., Smelror, M., Larsen, E., Andreassen, K., Eidvin, T., and Vorren, T., 2009. A new Plio-Pleistocene ice sheet model for the Svalbard/Barents Sea region. Quat Sci Rev, 28:812–829.

Ljones, F., Kuwano, A., Mjelde, R., Breivik, A., Shimamura, H., Murai, Y. and Nishimura, Y., 2004. Crustal transect from the North Atlantic Knipovich

Ridge to the Svalbard Margin west of Hornsund. Tectonophysics, 378: 17-41.

Lundin, E. and Doré, A.G., 2002. Mid-Cenozoic post-breakup deformation in the passive margins bordering the Norwegian–Greenland Sea. Marine and Petroleum Geology, 19(1): 79-93.

Macdonald, K.C., 1982. Mid-Ocean Ridges: Fine Scale Tectonic, Volcanic and Hydrothermal Processes Within the Plate Boundary Zone. Annual Reviews in Earth and Planetary Sciences, 10(1): 155-190.

Macdonald, K., Scheirer, D.S. and Carbotte, S.M., 1991. Mid-Ocean Ridges: Discontinuities, Segments and Giant Cracks. Science, 253(5023): 986-994.

Mjelde, R., Breivik, A.J., Elstad, H., Ryseth, A., Skilbrei, J.R., Opsal, J.G., Shimamura, H., Murai, Y., and Nishimura, Y., 2002a. Geological development of the Sørvestsnaget Basin, SW Barents Sea, from ocean bottom seismic, surface seismic and potential field data. Norwegian J. Geol., 82: 183–202.

Mjelde, R., Raum, T., Myhren, B., Shimamura, H., Murai, Y., Takanami, T., Karpuz, R., and Næss, U., 2005. Continent-ocean transition on the Vøring Plateau, NE Atlantic, derived from densely sampled ocean bottom seismometer data. J Geophys Res., 110:B05101.

Mjelde, R., Faleide, J.I., Breivik, A.J. and Raum, T., 2009. Lower crustal composition and crustal lineaments on the Vøring Margin, NE Atlantic: a review, Tectonophysics, 472(1–4): 183–193.

Michael, P.J., Langmuir, C., Dick, H.J.B., Snow, J.E., Goldstein, S.L., Graham, D.W., Lehnert, K., Kurras, G.J., Jokat, W., Muhe, R., and Edmonds, H.N., 2003. Magmatic and amagmatic seafloor generation at the ultraslow-spreading Gakkel ridge. Arctic Ocean: Nature, 423: 956–961.

Morgan W.J., 1971. Convection plumes in the lower mantle. Nature 230: 42-43.

Mourad B., 2006. Structure and evolution of the SW Barents Sea basin province Master thesis.

Nyland, B., Jensen, L. N., Skagen, J. I., Skarpnes, 0. and Vorren, T., 1992. Tertiary uplift and erosion in the Barents Sea; magnitude, timing and consequences. In: Structural and Tectonic Modeiling and its Application to Petroleum Geology (Eds R. M. Larsen et al.), Norwegian Petrol. Sot. Spec. Publ. No. 1, Elsevier, Amsterdam, pp. 153-162.

Nøttvedt, A., Cecchi, M., Gjelberg, J.G., Kristensen, S.E., Lønøy, A., Rasmussen, E., Skott, P.H. and Van Veen, P.M. 1992: Svalbard – Barents Sea correlation: a short review. In Vorren, T.O, Bergsager, E., Dahl- Stamnes, Ø.A., Holter, E., Johansen, B., Lie, E. & Lund, T.B. (eds.): Arctic Geology and Petroleum Potential, 363–375. Norwegian Petroleum Society Special Publication 2, Elsevier,Amsterdam.

Okino, K., Curewitz, D., Asada, M., Tamaki, K., Vogt, P. and Crane, K., 2002. Preliminary analysis of the Knipovich Ridge segmentation: influence of focused magmatism and ridge obliquity on an ultraslow spreading system. Earth and Planetary Science Letters, 202(2): 275-288.

Ottesen D., Dowdeswell J.A., and Rise L., 2005. Submarine landforms and the reconstruction of fast-flowing ice streams within a large Quaternary ice sheet: the 2500- km-long Norwegian–Svalbard margin (57°– 80° N). Geological Society of America Bulletin 117(7/8): 1033–1050.

Pidwirny, M., 2006. "Structure of the Earth". Fundamentals of Physical Geography, 2nd Edition. www.physicalgeography.net/fundamentals/10h.html.

Planke, S., Symonds, P., Alvestad, E. and Skogseid, J., 2000. Seismic volcanostratigraphy of large-volume basaltic extrusive complexes on rifted margins. Journal of Geophysical Research, 105: 19335–19351.

Reksnes, P. A. and Vagnes, E., 1985. Evolution of the Greenland Sea and Eurasia Basin Cand. Scient. Thesis, University of Oslo, 136 pp.

Ritzmann, O., and Faleide, J., I., 2007. Caledonian basement of the western Barents Sea. Tectonics, 26: TC5014.

Roberts, D. G., Hunter, P. M., and Laughton, A. S., 1979. Bathymetry of the northeast Atlantic continental margin around the British Isles. Deep Sea Researches, 26A: 417-428.

Rønnevik, H.C., 1981. Geology of the Barents Sea. In: L.V. llling and G.D. Hobson (Editors). Petroleum Geology of the Continental Shelf of North-West Europe. Inst. Pet., London, pp. 395-406.

Rønnevik, H.C. and Jacobsen, H.P., 1984. Structural highs and basins in the western Barents Sea. In Spencer, A.M.,Holter, E., Johnsen, S.O., Mørk, A., Nysæther, E., Songstad, P. & Spinnangr, Å. (eds.): Petroleum Geology of the North European Margin, 19–32. Norwegian Petroleum Society, Graham and Trotman, London.

Rudnick, R. I., and Fountain, D. M., 1995. Nature and composition of the continental crust: a lower crustal perspective: Reviews in Geophysics, 33: 267–310.

Ruppel, C., 1995. Extensional processes in continental lithosphere. Journal of Geophysical Research, 100: 24187– 24215.

Schilling, J.G., Kingsley, R., Fontignie, D., Poreda, R., and Xue, S., 1998. Dispersion of the Jan Mayen and Iceland mantle plumes in the Arctic: a He-Pb-Nd-Sr isotope tracer study of basalts from the Kolbeinsey, Mohns and Knipovich Ridges. J Geophys Res, 104:10543-10569.

Sclater, J. G., and J. Francheteau, 1970. The implications of terrestrial heat flow observations on current tectonic and geochemical models of the crust and upper mantle of the Earth. Geophys. J. R. Astron. Soc., 20: 509–542.

Solheim, A., Faleide, J.I., Andersen, E.S., Elverhøi, A., Forsberg, C.F., Vanneste, K., Uenzelmann-Neben, G., and Channell, J.E.T., 1998. Late Cenozoic seismic stratigraphy and glacial geological development of the East Greenland and Svalbard–Barents Sea continental margins. Quat Sci Rev, 17:155–184.

Spencer, A. M., Home, P. C. and Berglund, L. T., 1984. Tertiary structural development of the western Barents Shelf. In: Petroleum Geology of the North European Margin (Ed. A. M. Spencer), Graham and Trotman, London, pp. 199-209.

Spudich, P. and Orcutt, J., 1980. A new look at the seismic velocity structure of the oceanic crust. Rev. Geophys. Space Phys., 18: 627-645.

Stroup, J. G., and Fox, P. J., 1981. Geologic investigations in the Cayman Trough: Evidence for thin crust along the mid-Cayman rise. J. geol., 89, 395-420.

Sættem, J., Poole, D.A.R., Ellingsen, L., and Sejrup, H.P., 1992. Glacial geology of outer Bjørnøyrenna, southwestern Barents Sea. Marine Geology, 103 : 15-51.

Sun, S.S., Nesbitt, R.W., and Sharaskin, A.Y., 1979, Geochemical characteristics of mid-ocean ridge basalts. Earth and Planetary Science Letters, 44(1): 119–138.

Talwani, M. and Eldholm, O., 1977. The evolution of the Norwegian- Greenland Sea: recent results and outstanding problems. Geol. Soc. Am. Bull., 88**:** 969–999.

Torsvik, T.H., Mosar, J. and Eide, E.A., 2001. Cretaceous-Tertiary geodynamics: a North Atlantic exercise. Geophysical Journal International, 146(3): 850-866.

White, R.S. and McKenzie, D., 1989. Magmatism at rift zones: the generation of volcanic continental margins and flood basalts. J. geophys. Res., 94**,** 7685–7729.

WHITE, R.S., MCKENZIE, D. & O`NIONS, R.K. 1992. Oceanic crustal thickness from seismic measurements and rare earth element inversions. J. Geophys. Res., 97: 19683-19715.

Wilkens, R. H., Fryer, G. J. and Karsten, J., 1991. Evolution of porosity and seismic structure of upper oceanic crust: Importance of aspect ratios. J. Geophys. Res., 96(17): 981–17,995.

Worsley, D., Agdestein, T., Gjelberg, J.G., Kirkemo, K., Mørk, A., Nilsson, I., Olaussen, S., Steel, R.J. and Stemmerik, L., 2001. The geological evolution of Bjørnøya, Arctic Norway: implications for the Barents Shelf. Norsk Geol Tidsskr., 81:195–234.

Zelt, C.A. and Forsyth, D.A., 1994. Modeling wide-angle seismic data for crustal structure: Southeastern Grenville Province. Journal of Geophysical Research, 99(11): 687–11.

Zelt, C.A., 1999. Modelling strategies and model assessment for wide-angle seismic traveltime data. Geophys. J. Int., 139(1): 183-204.

APPENDIX

The following pages have the plots of the traced rays through the model for each OBS. Their plots, where calculated rays are overlain the picks, can be comparison between the picks and the rays.

OBS 2

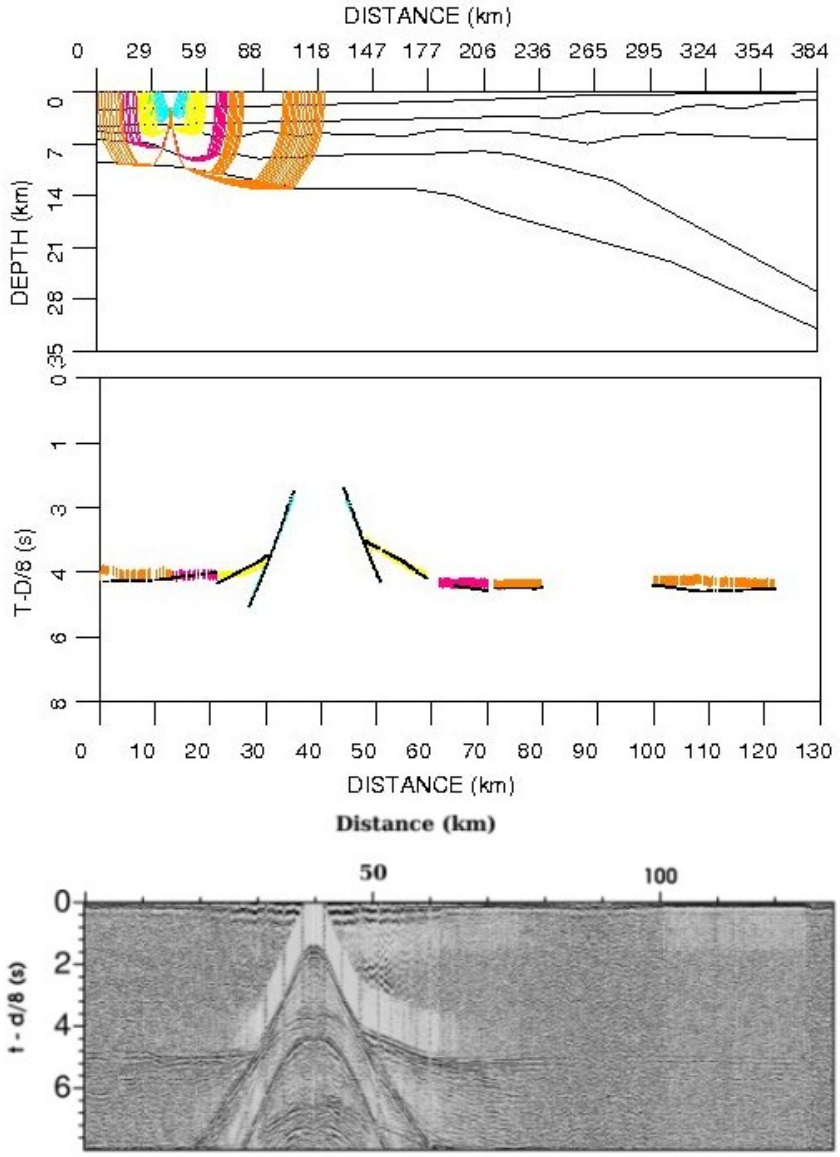

Figure A.1: Upper plot shows the Rays traced through the model, at the middle plot black lines show calculated rays and colors show the picks from Rayinvr, and lower plot displays seismogram of OBS 2.

OBS 3

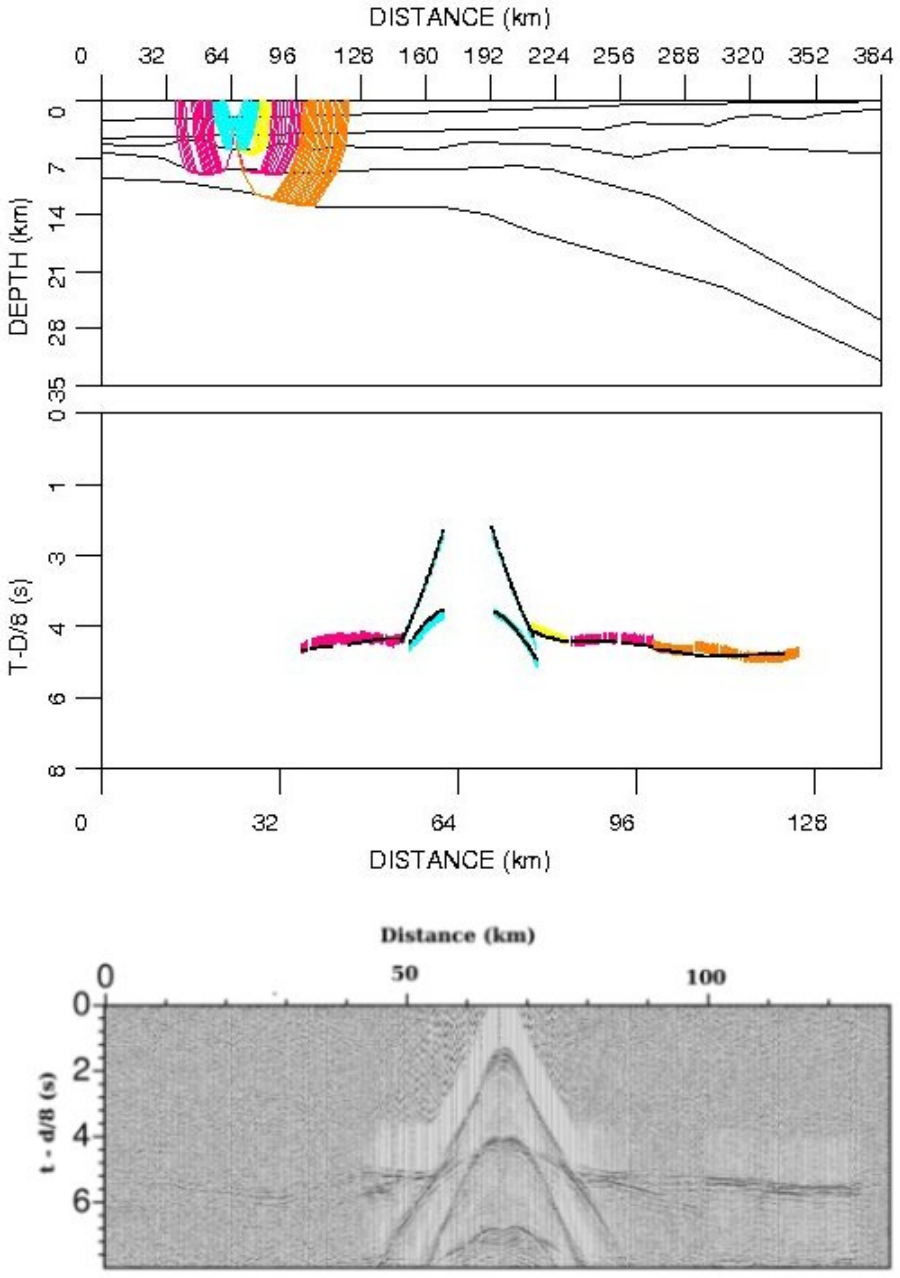

Figure A.2: Upper plot shows the Rays traced through the model, at the middle plot black lines show calculated rays and colors show the picks from Rayinvr, and lower plot displays seismogram of OBS 3.

OBS4

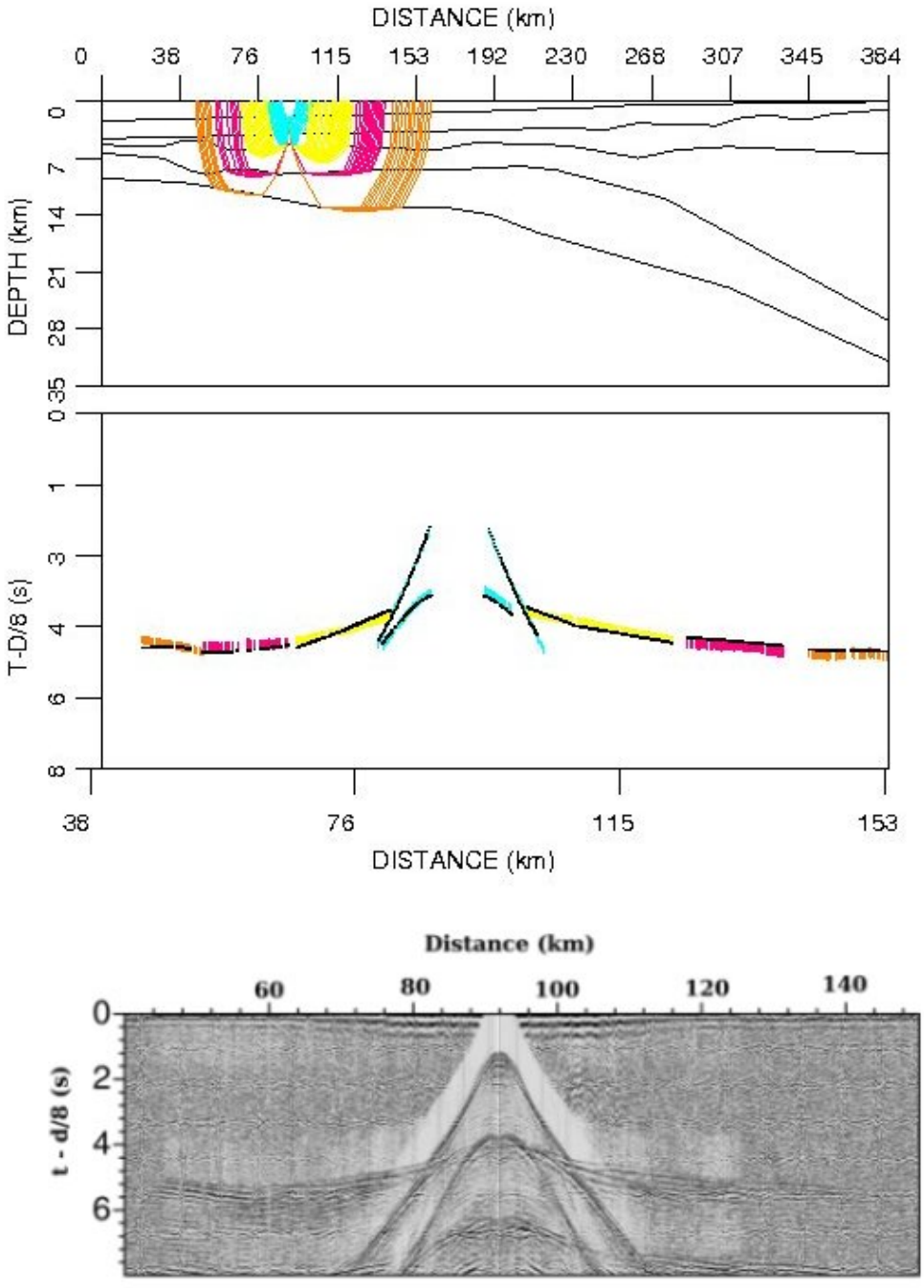

Figure A.3: Upper plot shows the Rays traced through the model, at the middle plot black lines show calculated rays and colors show the picks from Rayinvr, and lower plot displays seismogram of OBS 4.

OBS5

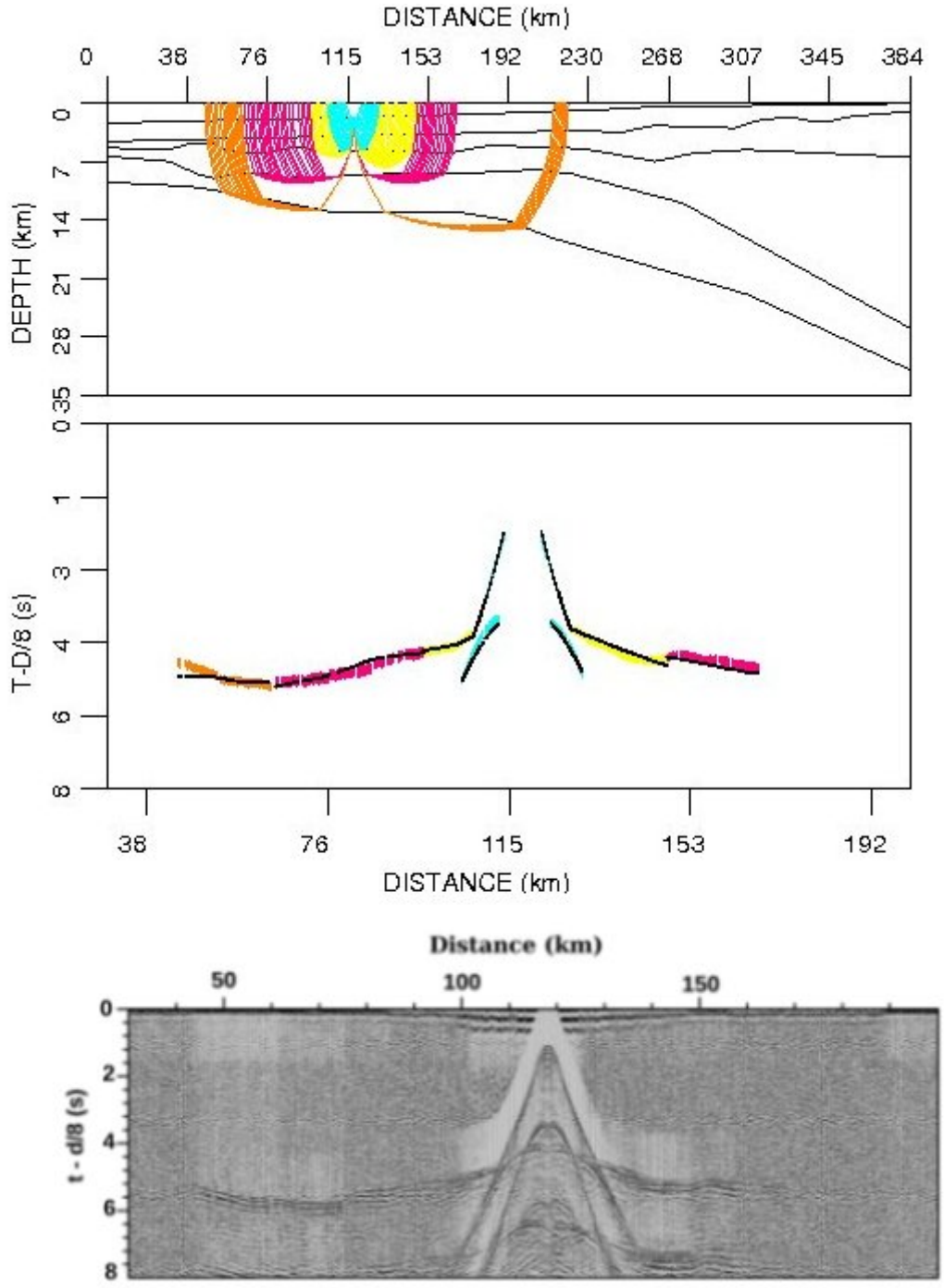

Figure A.4: Upper plot shows the Rays traced through the model, at the middle plot black lines show calculated rays and colors show the picks from Rayinvr, and lower plot displays seismogram of OBS 5.

OBS7

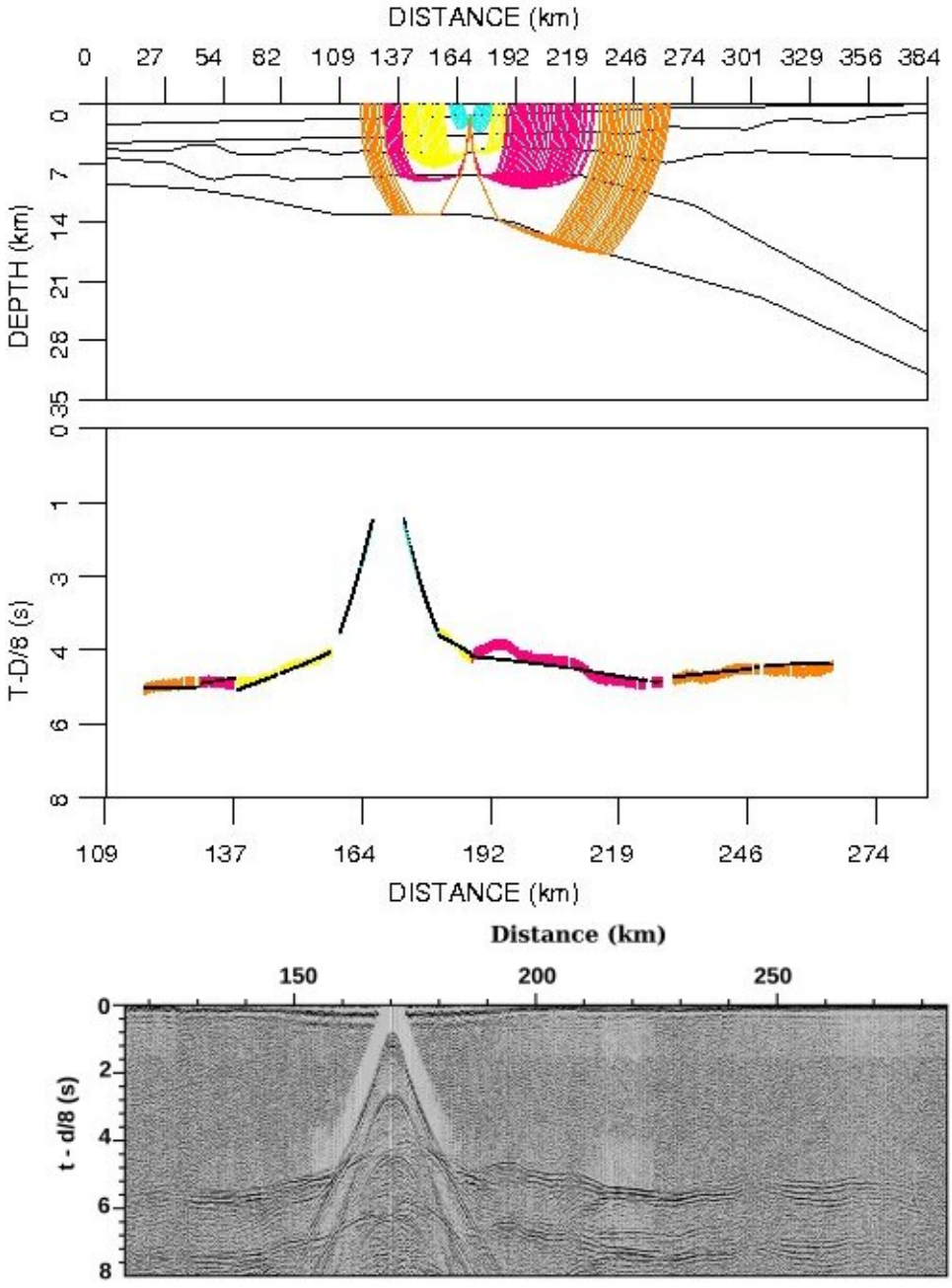

Figure A.5: Upper plot shows the Rays traced through the model, at the middle plot black lines show calculated rays and colors show the picks from Rayinvr, and lower plot displays seismogram of OBS 7.

OBS 8

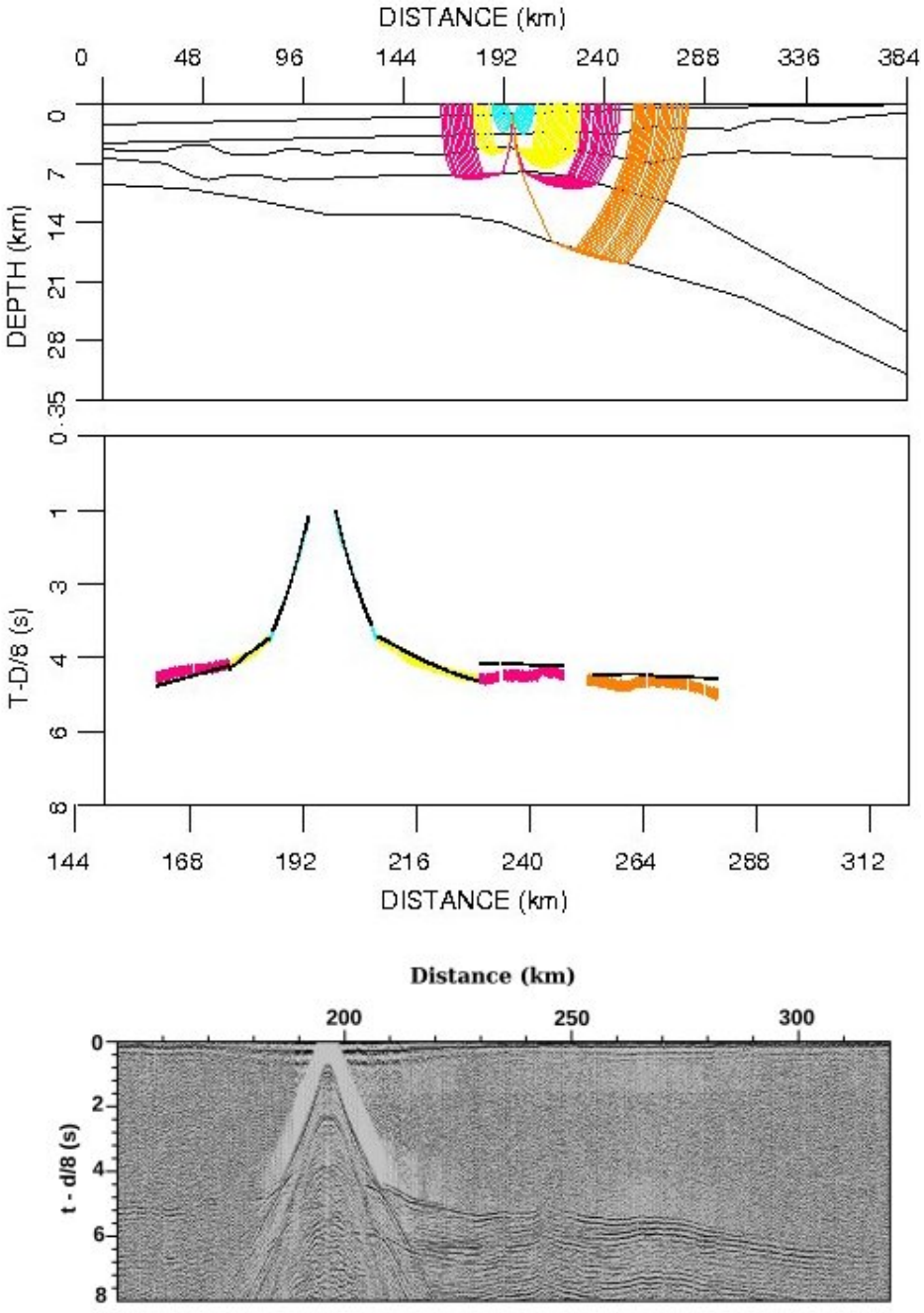

Figure A.6: Upper plot shows the Rays traced through the model, at the middle plot black lines show calculated rays and colors show the picks from Rayinvr, and lower plot displays seismogram of OBS 8.

OBS 9

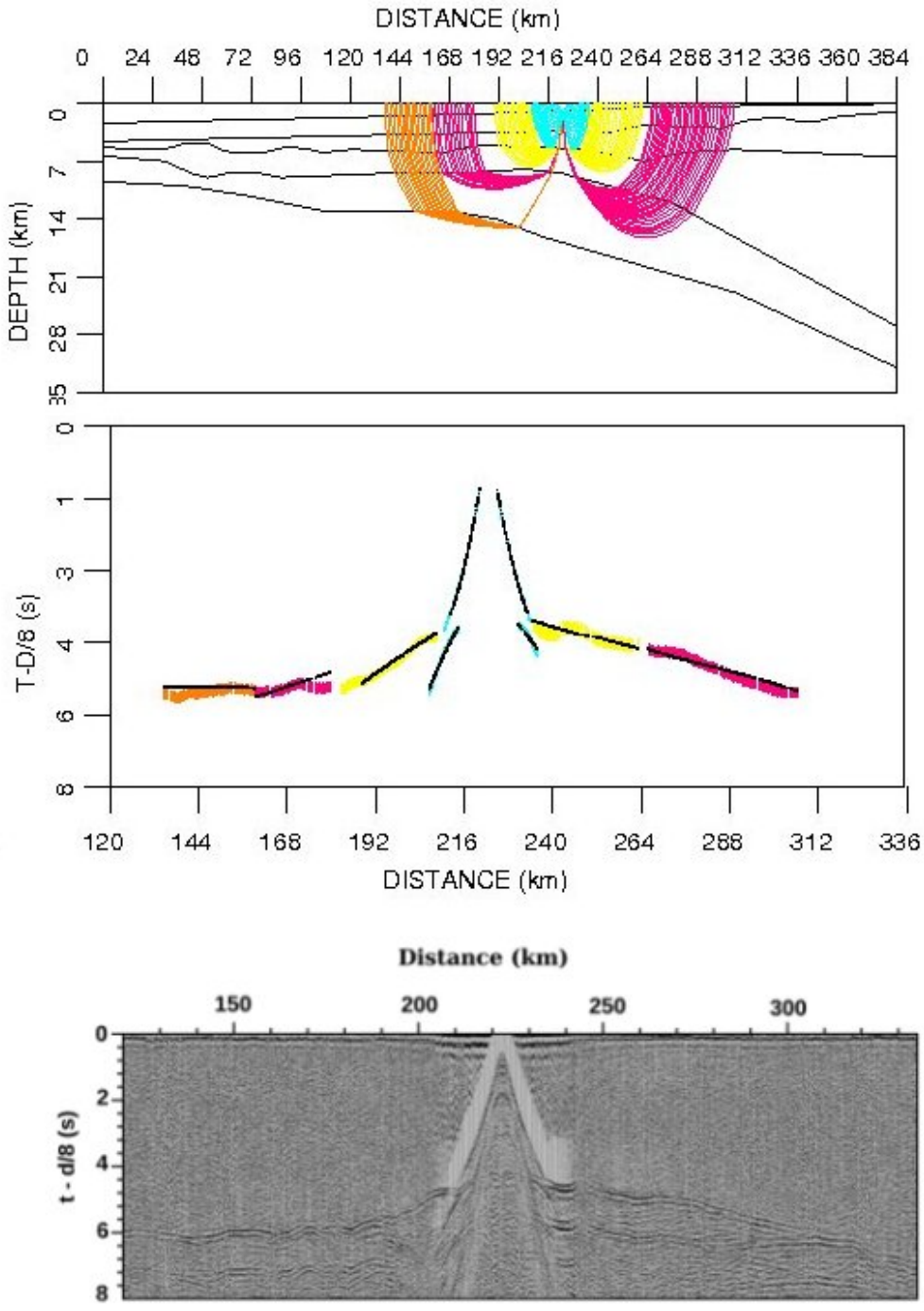

Figure A.7: Upper plot shows the Rays traced through the model, at the middle plot black lines show calculated rays and colors show the picks from Rayinvr, and lower plot displays seismogram of OBS 9.

OBS 10

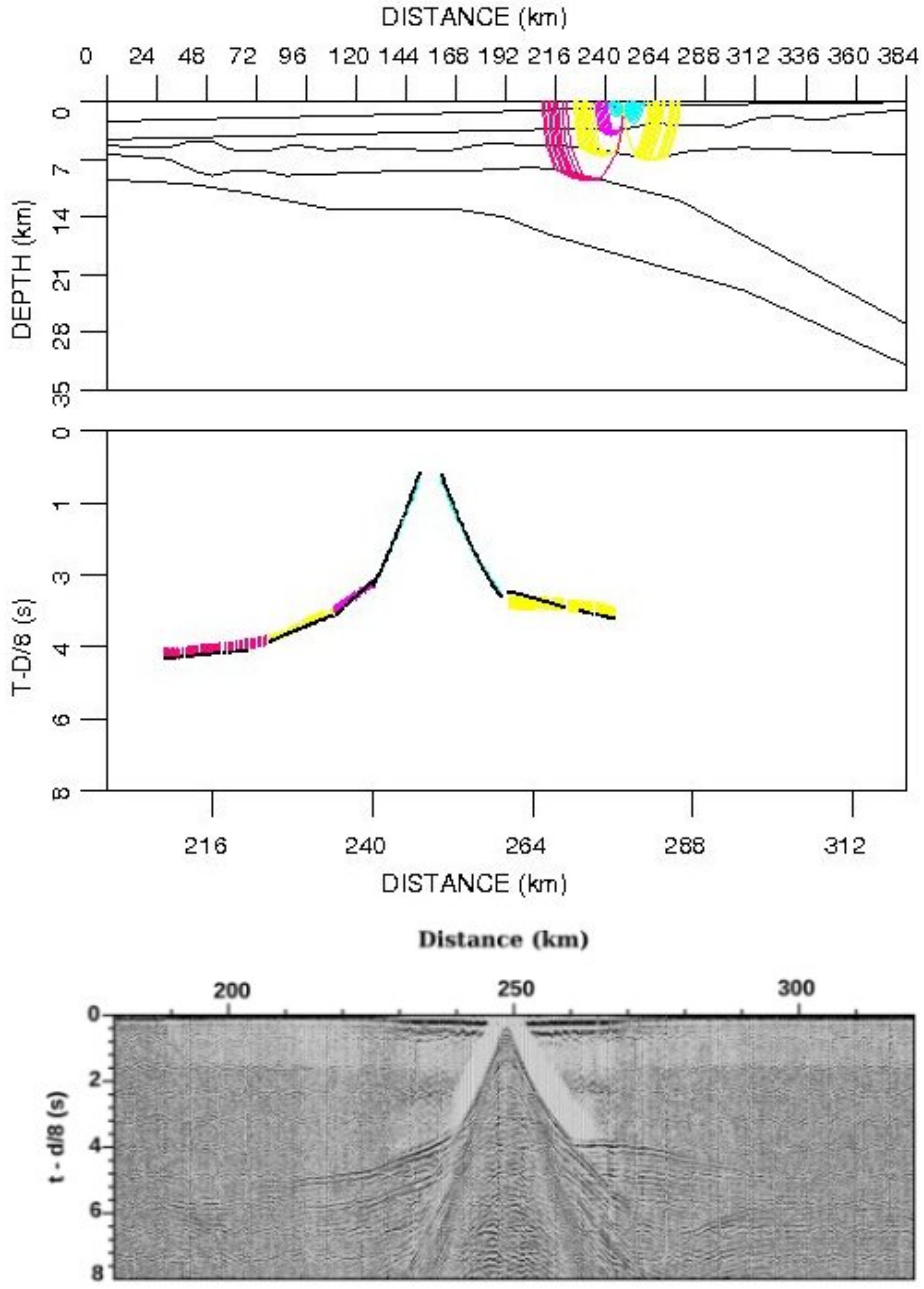

Figure A.8: Upper plot shows the Rays traced through the model, at the middle plot black lines show calculated rays and colors show the picks from Rayinvr, and lower plot displays seismogram of OBS10.

OBS 12

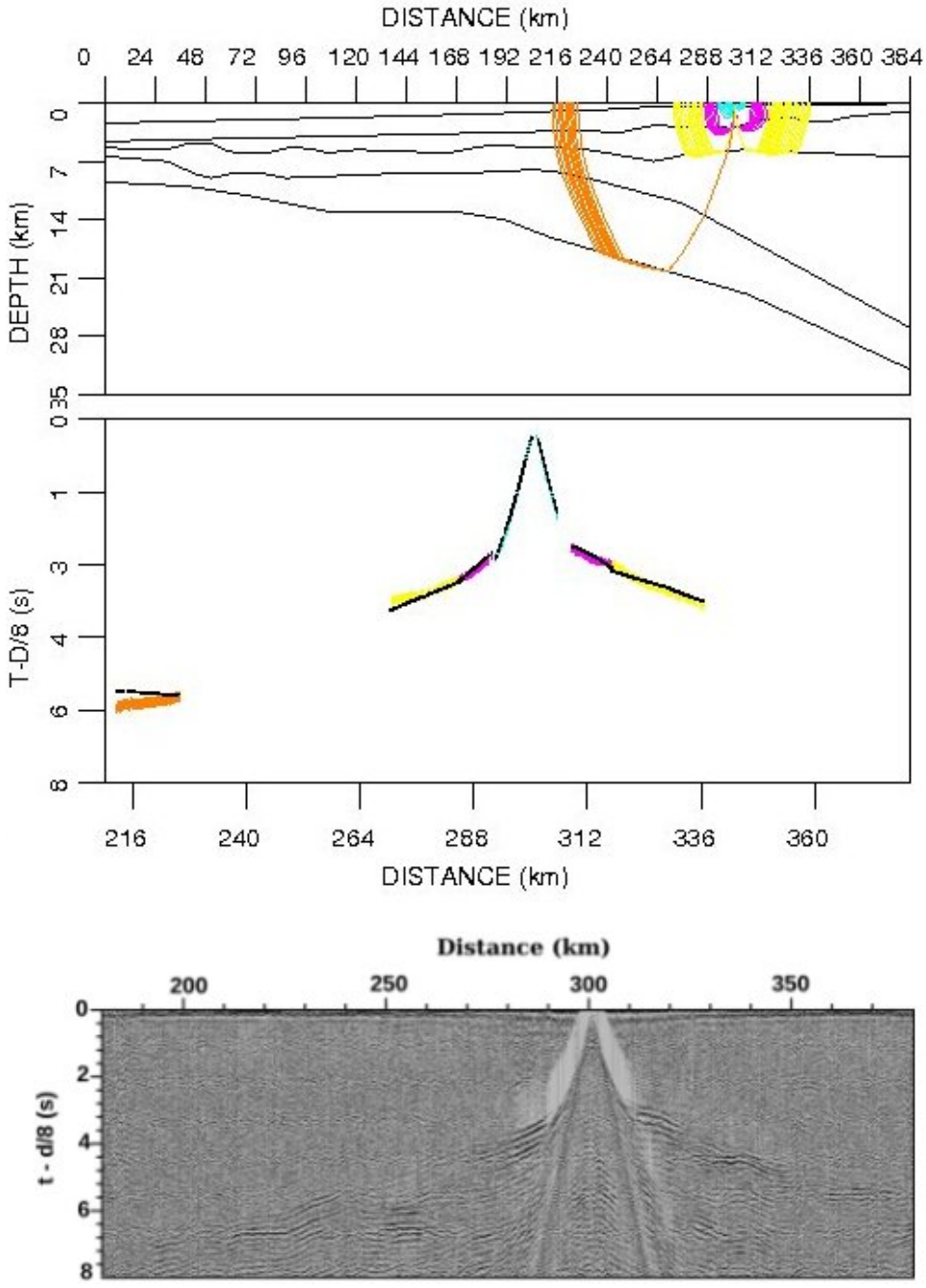

Figure A.9: Upper plot shows the Rays traced through the model, at the middle plot black lines show calculated rays and colors show the picks from Rayinvr, and lower plot displays seismogram of OBS12.

OBS 13

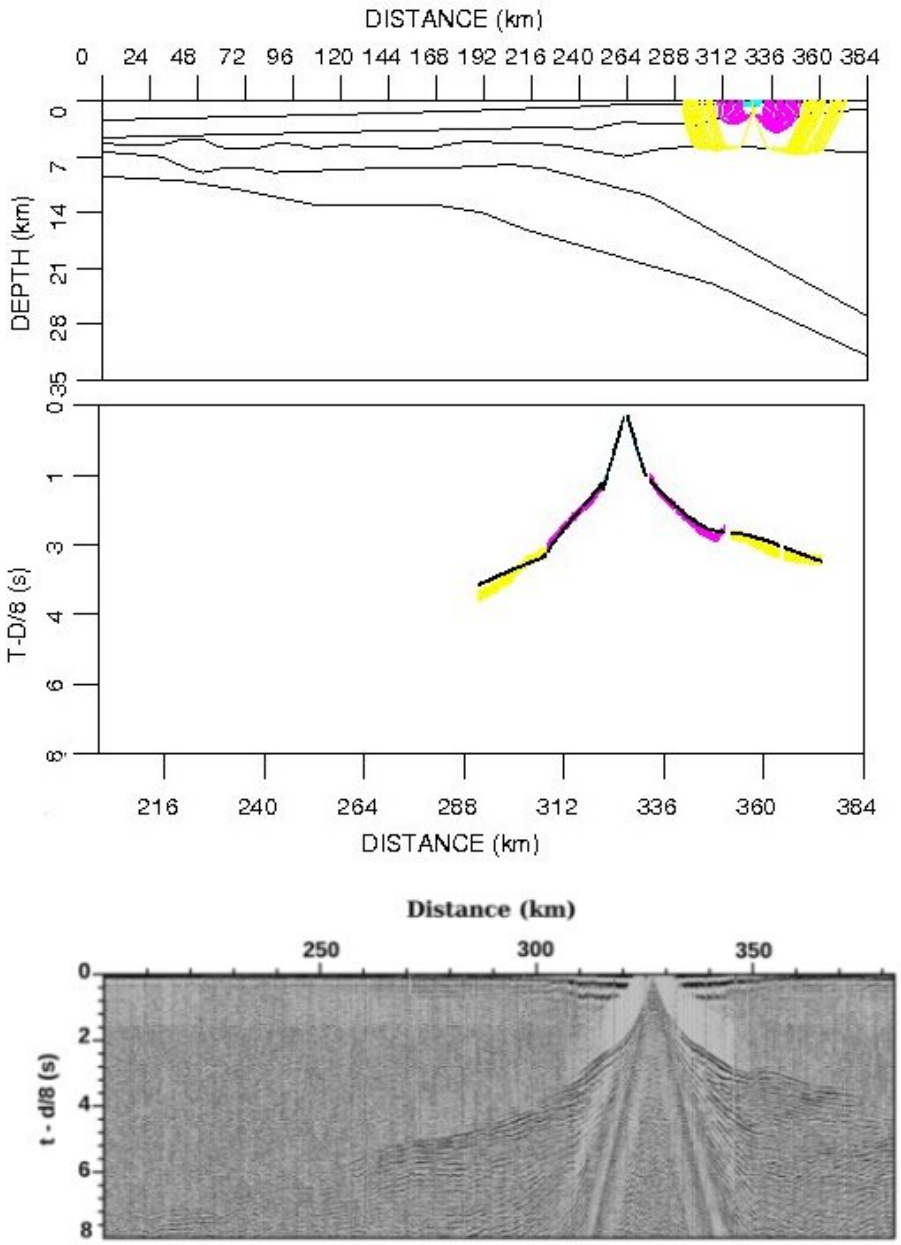

Figure A.10: Upper plot shows the Rays traced through the model, at the middle plot black lines show calculated rays and colors show the picks from Rayinvr, and lower plot displays seismogram of OBS13.

OBS 14

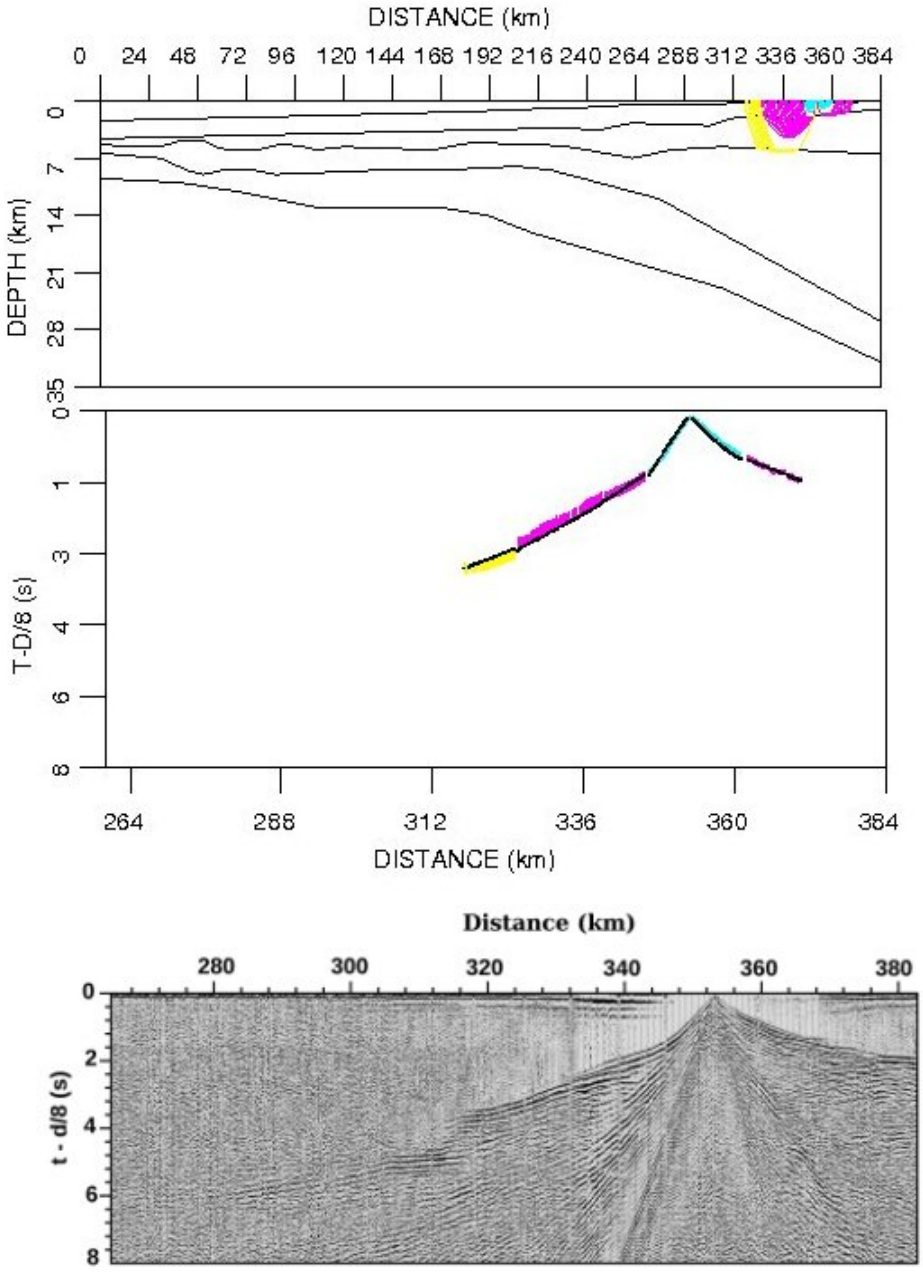

Figure A.11: Upper plot shows the Rays traced through the model, at the middle plot black lines show calculated rays and colors show the picks from Rayinvr, and lower plot displays seismogram of OBS14.

OBS 15

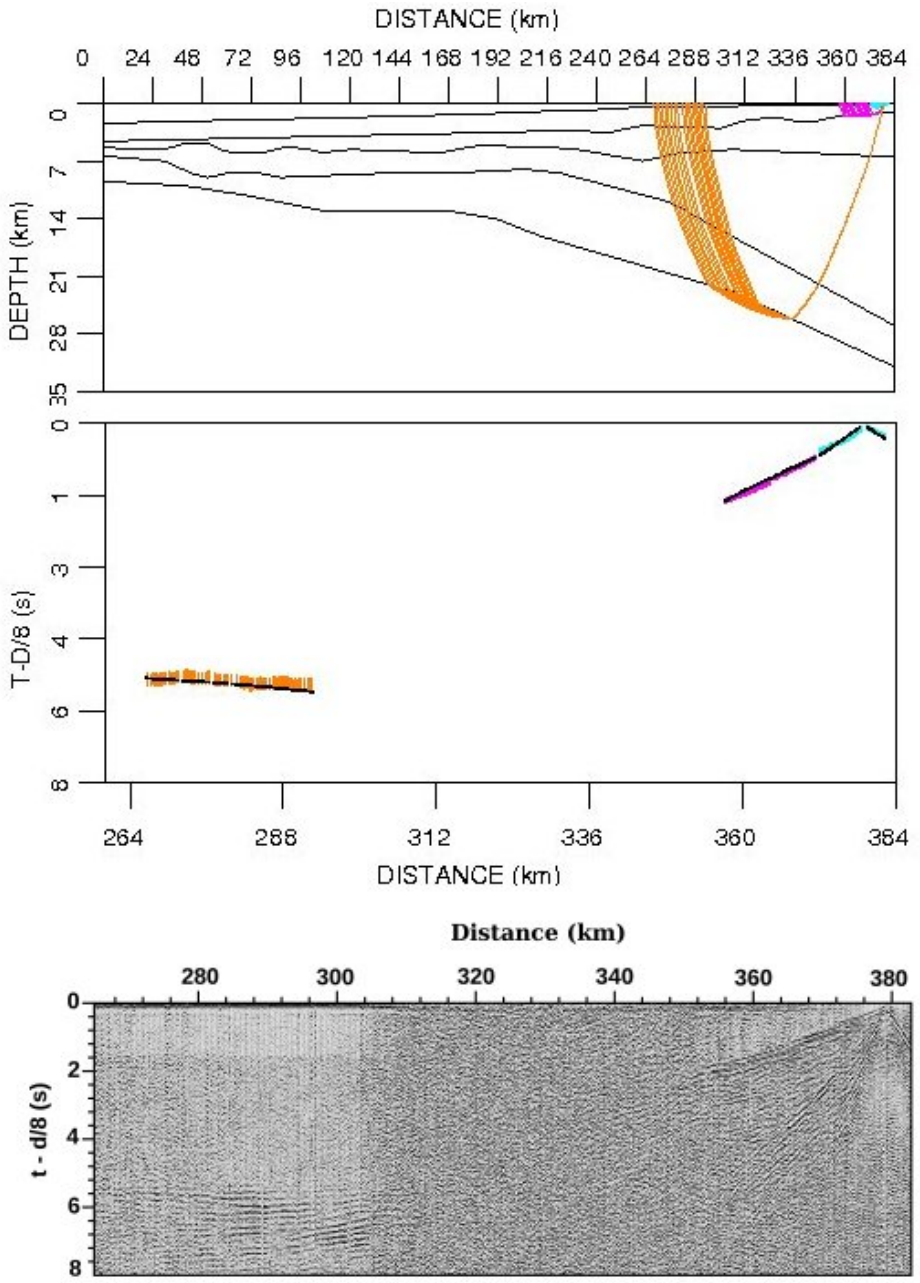

Figure A.12: Upper plot shows the Rays traced through the model, at the middle plot black lines show calculated rays and colors show the picks from Rayinvr, and lower plot displays seismogram of OBS15.